REFERENCES

Different Temporal and Spatial Gene Expression Patterns Occur during Anther Development

Anna M. Koltunow, Jessie Truettner,[1] Kathleen H. Cox,[2] Marco Wallroth,[3] and Robert B. Goldberg[4]

Department of Biology, University of California, Los Angeles, California 90024-1606

We studied the temporal and spatial regulation of three mRNA sequence sets that are present exclusively, or at elevated levels, in the tobacco anther. One mRNA set accumulates in the tapetum and decays as the tapetum degenerates later in anther development. The second mRNA set accumulates after the tapetal-specific mRNAs, is localized within the stomium and connective, and also decays as these cell types degenerate during anther maturation. The third mRNA sequence set persists throughout anther development and is localized within most anther tissues. A tapetal-specific gene, designated as TA29, was isolated from a tobacco genome library. Runoff transcription studies and experiments with chimeric β-glucuronidase and diphtheria toxin A-chain genes showed that the TA29 gene is regulated primarily at the transcriptional level and that a 122-base pair 5' region can program the tapetal-specific expression pattern. Destruction of the tapetum by the cytotoxic gene had no effect on the differentiation and/or function of surrounding sporophytic tissues but led to the production of male-sterile plants. Together, our studies show that several independent gene expression programs occur during anther development and that these programs correlate with the differentiated state of specific anther cell types.

INTRODUCTION

Reproductive processes in higher plants take place within two specialized floral organ systems, the stamen and the pistil (Esau, 1977; Raven et al., 1986; Goldberg, 1988; Drews and Goldberg, 1989). The anther compartment of the stamen contains diploid cells that undergo meiosis to form haploid microspores that differentiate into the pollen grains or male gametophyte (Vasil, 1967; Esau, 1977; Raven et al., 1986). By contrast, sporogenous cells within the ovary of the pistil ultimately lead to the production of the female gametophyte, or embryo sac, that contains the egg cell (Esau, 1977; Raven et al., 1986). Pollination is required to transfer pollen grains containing the sperm cells to the stigma of the pistil so that fertilization can occur in the embryo sac (Esau, 1977; Raven et al., 1986).

Stamens are differentiated from primordia that are specified within the floral meristem following the transition from a vegetative to a flowering pathway (Esau, 1977; Raven et al., 1986). Stamen primordia specification depends upon the action of several genes (Bowman et al., 1989; Meyerowitz et al., 1989; Carpenter and Coen, 1990), some of

which may encode transcriptional activator proteins (Sommer et al., 1990; Yanofsky et al., 1990). Following stamen primordia initiation, several highly specialized anther tissues are differentiated from cell lineages present in the floral meristem (Satina and Blakeslee, 1941) and are responsible for carrying out nonreproductive functions (e.g., support, dehiscence) and reproductive functions (e.g., spore and gamete formation).

The molecular processes that are responsible for specifying functionally distinct anther cell types after primordia initiation are not well understood. Previously, we used RNA-excess DNA/RNA hybridization experiments to show that approximately 25,000 diverse genes are expressed in the tobacco anther (Kamalay and Goldberg, 1980). Comparisons of tobacco organ system mRNA and nuclear RNA populations showed that about 10,000 mRNAs are anther specific and are undetectable in the cytoplasm and nucleus of cells in other vegetative and floral organ systems (Kamalay and Goldberg, 1980, 1984). These findings suggest that the transcriptional activation of specific gene sets is required for the establishment and maintenance of differentiated cell types and functions during anther development.

In this paper, we describe the temporal and spatial expression patterns of several different anther-specific genes. Our results show that distinct gene expression programs occur during anther development and that these programs correspond with the differentiation of functionally

[1] Current address: Department of Cell Biology, University of Miami, Miami, FL 33101.
[2] Current address: Department of Microbiology, University of Tennessee, Memphis, TN 38163.
[3] Current address: Plant Cell Research Institute, San Carlos, CA 94070.
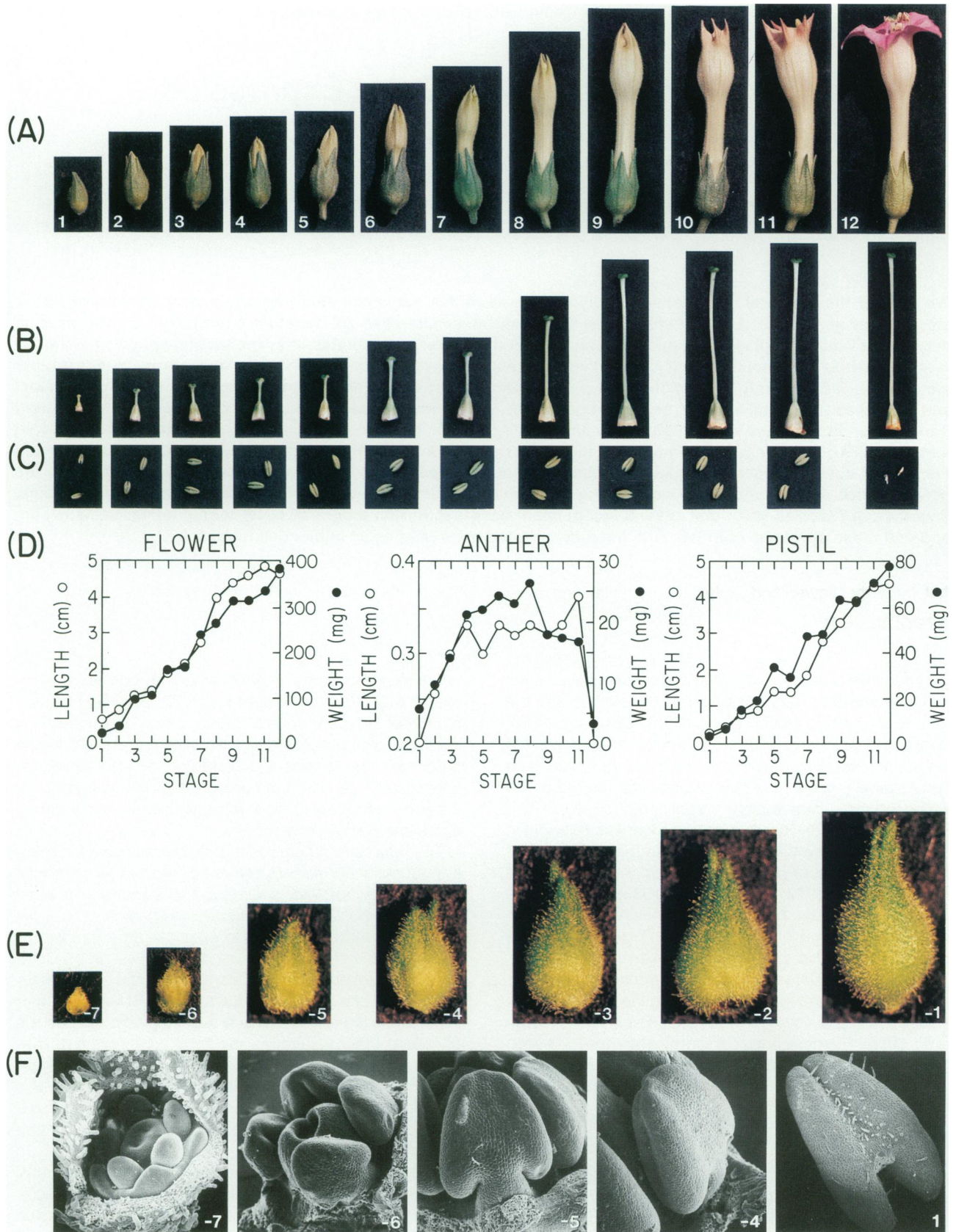[4] To whom correspondence should be addressed.

Figure 1. Tobacco Flower Development.

(A) Flower development from 8-mm bud to opening. Flower buds were divided into 12 stages on the basis of size [**(D)**] and morphological

distinct cell types. Transformation studies with one anther-specific gene, designated as TA29 (Mariani et al., 1990; Seurinck et al., 1990), demonstrated that sequences responsible for the transcriptional activation of this gene in the tapetum are localized within a 122-bp 5′ region. Destruction of the tapetum by a chimeric TA29 diphtheria toxin A-chain gene indicated that the tapetum is not required for the differentiation and/or function of other specialized cell types later in anther development.

RESULTS

Anther Development Has Two Distinct Phases

Previously, we divided tobacco flower development into 12 stages to provide reference points for the expression of genes in different floral organ systems (Goldberg, 1988). Figure 1A shows these stages, and the floral bud lengths and morphological markers used to describe each stage are summarized in Table 1. Figures 1B and 1C correlate each stage with the developmental state of the pistil and anthers. Measurements presented in Figure 1D indicate that both the flower bud (calyx plus corolla) and pistil increase in fresh weight and length continuously from stages 1 to 12. By contrast, the anthers increase in weight and length only until stage 5. These parameters remain relatively constant until stage 11 and then decrease precipitously when flower opening and anther dehiscence occur at stage 12 (Figures 1A and 1C).

We prepared transverse anther sections at each stage to correlate changes in external morphology (Figure 1C) with the presence of specific sporophytic tissues and cell types and with the presence of microspores and pollen grains. Bright-field photographs of representative anther

sections are shown in Figure 2A, and the major tissues present and developmental events that occurred from stages 1 to 12 are summarized in Table 1. At stage 1, all major anther tissues have been specified. These included the epidermis, endothecium, vascular bundle, connective, stomium, and tapetum. In addition, meiosis was finished and the microspores were bound together as tetrads in the pollen sac. Following stage 1, the pollen grains differentiated and the anther underwent a series of events leading to dehiscence and pollen release (Figure 2A and Table 1). For example, by stage 8, the tapetum was degenerated, the connective separating the pollen sacs had begun to degrade, and the anther wall showed signs of splitting in the stomium region (Figure 2A and Table 1). At stage 11, the connective was absent, the anther was bilocular, and pollen grains filled the locules (Table 1).

We characterized anthers at earlier developmental stages to determine when the major histodifferentiation events occurred. Figure 1E shows pictures of flower bud development before stage 1. We divided these buds into seven stages on the basis of both length (Table 1) and morphological markers observed in the scanning electron microscope (Figure 1F). Early flower bud stages were designated with a minus sign to indicate that they occurred before the completion of meiosis within the anther (Table 1).

The scanning electron micrographs shown in Figure 1F and the transverse sections shown in Figure 2A indicate that anther primordia were present in stage −7 flower buds and that the differentiation of specific anther tissues had begun. For example, archesporial cells, connective tissue, prevascular tissue, and epidermis were already visible at this developmental stage (Table 1). Between stages −7 and −1, the anther acquired its characteristic external shape (Figure 1F), all major anther tissues were differentiated (Table 1), and the microspore mother cells

---

Figure 1. (continued).

criteria (Table 1). Stage 1 was designated as the period when tetrads are present within the anther and corresponds to an 8-mm flower bud. Stage 12 was designated as the time of flower opening and anther dehiscence. The transition from stage 1 to stage 12 occurred over a 1-week period during the summer.
(B) Pistil development from stage 1 to stage 12. Pistil lengths and weights are presented in **(D)**.
(C) Anther development from stage 1 to stage 12. Anther lengths and weights are presented in **(D)**.
(D) Changes in organ system weight and length during flower development. Five flower buds were picked at each developmental stage, and their lengths and fresh weights were measured individually. Similar measurements were made for the anthers and pistil of each flower bud. Data points represent the mean of these five measurements. Anther fresh weights represent the collective weight of all five anthers within the flower bud.
(E) Flower development from 0.75-mm bud to 7-mm bud. Young flower buds were divided into seven stages on the basis of size and developmental events occurring within the anther (Table 1). Stage −7 was designated as the period when tissue differentiation begins in the anther primordium [**(F)**] and stage −1 was designated as the period just before the completion of meiosis within the anther (Figure 2 and Table 1). Stage −7, −6, −5, −4, −3, −2, and −1 flower buds averaged 0.75 mm, 1.5 mm, 3 mm, 4 mm, 5 mm, 6 mm, and 7 mm in length, respectively. The transition from stage −7 to stage −1 occurred over approximately 5 days. Photographs were taken using a dissecting microscope with a magnification factor of ×75.
(F) Scanning electron micrographs of anthers during the early stages of development. Flower buds at the designated stages were harvested, and their sepals and petals were removed to expose the anthers. The dissected flower buds were then photographed in the scanning electron microscope as outlined in Methods. Magnification factors for the stage −7, −6, −5, −4, and 1 anthers were ×170, ×120, ×120, ×125, and ×60, respectively.

Table 1. Major Events during Tobacco Anther Development

Flower			Anther	
Stage	Bud Length[a]	Morphological Markers[b]	Tissues Present[c]	Major Events and Morphological Markers[d]
−7	0.75	Petal and stamen primordia present; carpels forming; calyx almost closed.	E, V, A, C	Rounded primordium; tissue differentiation begun.
−6	1.5	Calyx closed; carpels not fused.	E, V, Sp, P, C	Intense mitotic activity in four corners; invagination of inner side.
−5	3	Carpels fused; stamen filaments elongated; petals equal in length with anthers.	E, En, T, V, MMC, C	Wall layers including endothecium and tapetum being formed; connective established.
−4	4	Anthers yellowish; petals enclose anthers; stigma forming.	E, En, T, V, MMC, C	Tapetum and pollen sacs distinct; inner and outer tapetum morphologically different; middle layer crushed.
−3	5	Style elongating; stamen filament extension continues; anthers below stigma.	E, En, T, V, MMC, C	Meiosis begins; callose deposition between microspore mother cells evident.
−2	6	Style clearly elongated; ovary expanded; anthers below stigma.	E, En, T, V, MMC, C, S	Meiosis in progress; tapetum large and multinucleate; stomium differentiation begins; thick callose walls between microspore mother cells.
−1	7	Petals approaching top of sepals.	E, En, T, V, MMC, C, S	Meiosis in progress; continued stomium differentiation.
1	8	Anthers and pistil fully differentiated and green.	E, En, T, V, TDS, C, S	Meiosis complete; microspores in tetrad; stomium differentiated; all sporophytic tissues formed.
2	11	Calyx opens slightly at top of bud.	E, En, T, V, Msp, C, S	Microspores separate.
3	14	Corolla emerges from calyx.	E, En, T, V, Msp, C, S	Tapetum shrunken; secondary thickening in outer wall layers; pollen grains begin to form.
4	16	Sepals completely separated at top of calyx.	E, En, T, V, Msp, C, S	Cells adjacent to stomium degenerated; tapetum degenerating.
5	20	Corolla tube bulge just inside calyx.	E, En, T, V, Msp, C, S	Secondary thickening in outer wall layers intensified.
6	22	Corolla tube bulge at tip of calyx.	E, En, T, V, Msp, C, S	Remnants of tapetum present; microspore nucleus dividing.
7	28	Corolla tube bulge above calyx; petals closed.	E, En, V, Msp, C, S	Degradation of connective tissue in stomium region.
8	39	Corolla elongating; petals green and slightly open.	E, En, V, Msp, C, S	Disruption of connective tissue separating pollen sac.
9	43	Corolla tube bulge enlarging; petal tips becoming pink.	E, En, V, Msp, C, S	Continued connective degradation.
10	45	Corolla limb beginning to open; petal tips pink.	E, En, V, Msp, S	Connective tissue almost fully degraded; pollen binucleate.
11	47	Corolla limb halfway open; stigma and anthers visible.	E, En, V, Msp, S	Anthers bilocular; connective absent; locules filled with mature pollen grains.
12	46	Flower open; anthers dehisced; corolla limb fully expanded and deep pink.	E, En, V, PG	Anthers dehisce along stomium; pollen released.

[a] Mean of five individual determinations expressed in millimeters. Data from stages 1 to 12 taken from those presented in Figure 1D.
[b] Major markers that can be used with bud length measurements to identify stage. Tube refers to the white elongated portion of the corolla; limb refers to the top pink corolla region where the petal tips are separated from each other (Figure 1A). Markers for stages −7 to −1 taken from the scanning electron micrographs (Figure 1F); markers for stages 1 to 12 were taken from visual inspection of buds (Figure 1A).
[c] A, archesporial cells; C, connective; E, epidermis; En, endothecium; MMC, microspore mother cells; Msp, microspores; P, parietal layer; PG, pollen grains; S, stomium; Sp, sporogenous cells; T, tapetum; TDS, tetrads; V, vascular tissue. Taken from bright-field photographs of transverse anther sections (Figures 2 and 14).
[d] Taken from bright-field photographs of transverse anther sections (Figures 2 and 14).

were undergoing meiosis (Figure 2A). Taken together, these data indicate that anther developmental stages can be correlated with floral bud lengths and that there are two major phases of anther development: phase 1—tissue differentiation, microspore mother cell specification, and meiosis (stages −7 to −1), and phase 2—growth, pollen grain differentiation, and tissue degeneration and dehiscence (stages 1 to 12).

Anther-Specific Clones Were Identified in an Anther cDNA Library

We constructed a stage 6 (Figures 1A and 1C) anther cDNA library and then screened this library for cDNA clones that represented mRNAs present exclusively, or at elevated levels, in the anther (see Methods). We used stage 6 anther mRNA to construct the library because our earlier solution DNA/RNA hybridization studies indicated that stage 6 anthers contain a large number of anther-specific mRNAs (Kamalay and Goldberg, 1980, 1984). We obtained 58 anther-specific cDNA clones out of a screen of 768 plasmids and then sorted 26 of these clones into groups by RNA gel blot and cross-hybridization analyses. Sixteen cDNA clones failed to cross-hybridize at a moderately stringent criterion (42°C, 50% formamide, 1 M Na⁺) and were designated as unique. The remainder were found to belong to four different cross-hybridizing groups.

Table 2 lists representative cDNA clones from three of the groups, as well as others that sorted into the unique category. DNA sequencing studies (Seurinck et al., 1990; J. Seurinck, J. Leemans, and R.B. Goldberg, unpublished results) showed that the TA32/36 and TA56/57 groups represented mRNAs encoding lipid transfer proteins (Bouillon et al., 1987; Takishima et al., 1988) and thiol endopeptidase proteins (Miller and Huffaker, 1982; Mitsuhashi and Minamikawa, 1989), respectively. In addition, the TA13/TA29 group represented mRNAs that encoded glycine-rich proteins with properties of cell wall proteins (Condit and Meagher, 1986; Keller et al., 1988; Varner and Cassab, 1988). By contrast, the unique anther cDNA clones sequenced to date (e.g., TA20, TA25, and TA26) failed to show relatedness to any known mRNA or protein.

We hybridized representative anther cDNA probes with gel blots containing floral and vegetative organ system mRNAs. As shown in Figure 3, all probes produced strong hybridization signals with anther mRNA. Prevalence estimates indicated that these mRNAs represented from 0.05% to 0.5% of the anther mRNA, depending upon the message (Table 2). In most cases, the cDNA probes failed to produce a detectable signal with heterologous organ mRNAs, even after the gel blots were exposed 50 times longer than that required to produce a weak anther signal. By contrast, three cDNA clones (TA20, TA26, TA4) produced signals with other mRNAs in addition to anther mRNA; however, in each case, the heterologous hybridi-

zation signal was at least 10-fold lower than that observed in the anther. In addition, each of these cDNA clones produced a distinct hybridization pattern with the heterologous mRNAs (Figure 3). For example, the TA20 probe hybridized with pistil and petal mRNAs, whereas the TA26 probe hybridized only with leaf mRNA. Taken together, these data indicate that we have identified several different anther-specific cDNA clones, that these clones represent relatively prevalent anther mRNAs, and that most of these mRNAs are either undetectable in other organ system mRNAs at our sensitivity level (e.g., TA13, TA29, TA36) or are present at a level at least 10-fold lower than that observed in the anther (e.g., TA4, TA20, TA26).

Gene Expression Is Temporally Regulated during Anther Development

We hybridized representative anther cDNA plasmids with mRNAs from different anther stages to determine whether their corresponding genes were regulated temporally during anther development. These plasmids included the eight listed in Table 2 in addition to 11 others. Figures 4A and 4B present the results of RNA dot blot studies, and Figure 4C shows duplicate RNA gel blot experiments with some of the same plasmids.

Three distinct gene expression patterns were observed. First, Figures 4A and 4C show that most anther mRNAs investigated accumulated coordinately between stages 1 and 4 and then their levels declined significantly after stage 6. These mRNAs included those encoding the glycine-rich proteins (TA13, TA29) and the lipid transfer proteins (TA32, TA36). Second, Figure 4B shows that the TA20 and TA25 mRNAs were present at relatively similar levels in all stages studied. Closer inspection of the data, however, indicated that these mRNAs increased slightly in prevalence between stages 2 and 3 (Figure 4B). Finally, Figures 4B and 4C show that the thiol endopeptidase mRNAs (TA56, TA57) accumulated between stages 1 and 6, remained relatively constant until stage 8, and then declined to low levels before dehiscence at stage 11. Together, these data indicate that many anther-specific genes are regulated temporally and that there are timing differences in anther gene expression patterns.

Gene Expression Is Spatially Regulated during Anther Development

We hybridized single-stranded ³⁵S-RNA probes with anther sections in situ (see Methods) to correlate the temporal gene expression patterns observed during anther development (Figure 4) with the presence of specific anther tissues and cell types (Figure 2 and Table 1).
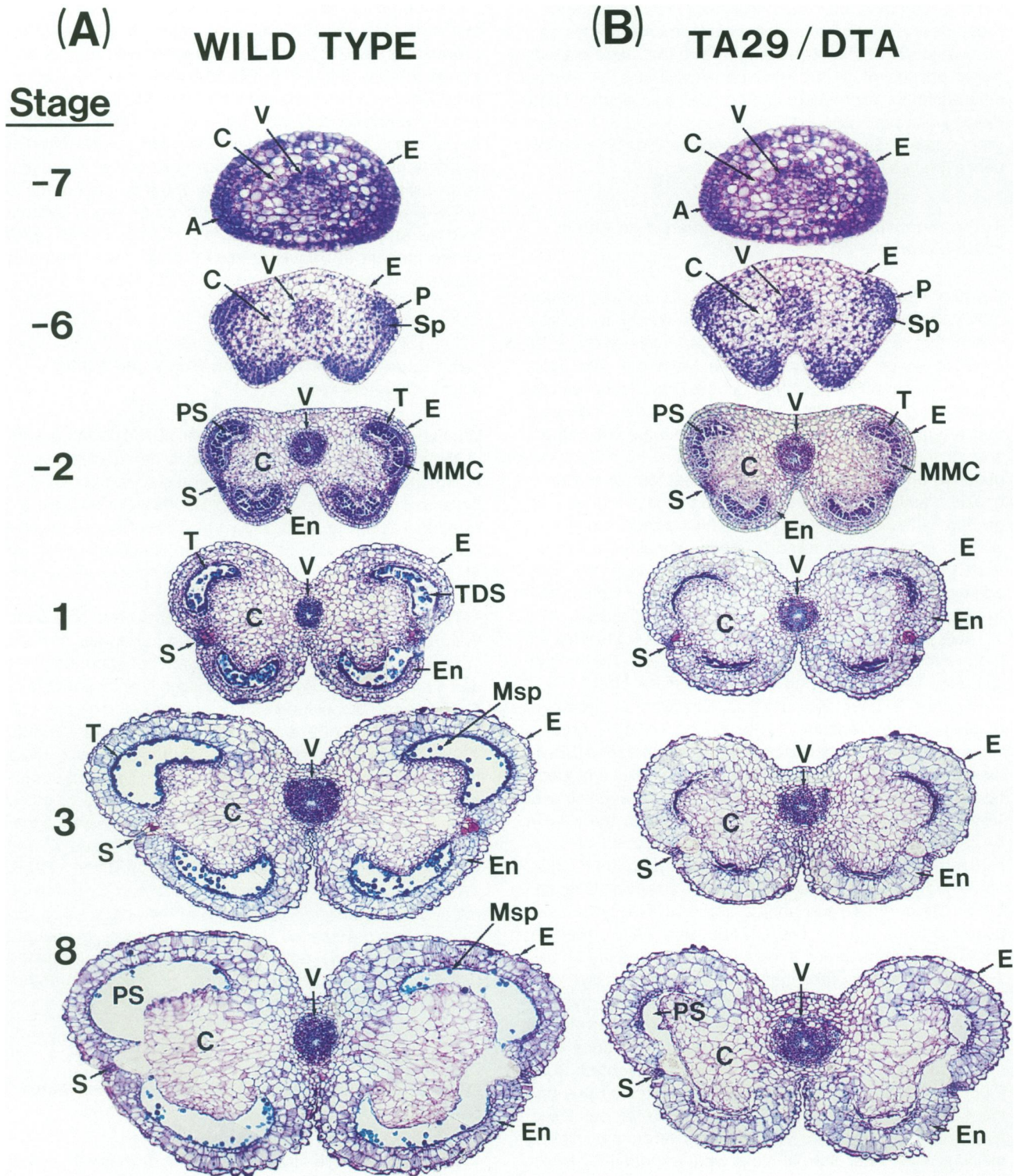
Figure 2. Bright-Field Photographs of Tobacco Anther Development in Untransformed Plants and Plants Transformed with a Chimeric TA29/DTA Gene.

Anthers at the designated stages were fixed, embedded with paraffin, and sliced into 10-μm transverse sections as described in Methods. The fixed sections were stained with toluidine blue and photographed with bright-field illumination. A, archesporial cells; C, connective; E,

Table 2. Anther-Specific mRNAs

mRNA	Size[a]	Prevalence[b]	Protein Encoded[c]
TA13[d]	1.1, 1.2	0.4	Glycine-rich
TA20[e]	0.6	0.5	Unknown
TA25[e]	0.7	0.2	Unknown
TA26[e]	0.6, 0.7	0.2	Unknown
TA29[d]	1.1, 1.2	0.2	Glycine-rich
TA32[f]	0.6, 0.7	0.05	Lipid transfer
TA36[f]	0.6, 0.7	0.05	Lipid transfer
TA56[g]	1.5	0.05	Thiol endopeptidase

[a] Taken from Figure 3.

[b] Percentage of stage 3 anther polysomal poly(A) mRNA. Estimated relative to calibrated RNA standards. The TA13 and TA29 mRNA prevalences were estimated using mRNA-specific oligonucleotide probes.

[c] Translation of DNA sequence (Seurinck et al., 1990), or highest identity score with proteins in the GenBank.

[d] Different members of the same family. TA13 and TA29 mRNAs are 90% similar at the nucleotide level (J. Seurinck, J. Leemans, and R.B. Goldberg, unpublished data).

[e] Not significantly similar at the nucleotide level to each other or to the other mRNAs listed in this table (J. Seurinck, J. Leemans, and R.B. Goldberg, unpublished data).

[f] Different members of the same gene family. TA32 and TA36 mRNAs are 63% similar at the nucleotide level (J. Seurinck, J. Leemans, and R.B. Goldberg, unpublished data), and their cDNA plasmids only weakly hybridize at a moderately stringent criterion (42°C, 50% formamide, 1.2 M Na$^+$).

[g] The TA56 and TA57 cDNA plasmids (Figure 4B) cross-hybridize at a moderately stringent criterion.

Several Different Anther mRNAs Are Localized within the Tapetum

Figure 5 shows the localization patterns of the TA26, TA29, and TA32 mRNAs (Table 2). As seen in Figures 5A to 5C, no hybridization grains above background were observed with the TA29 mRNA control probe. By contrast, Figures 5D to 5L show that the TA26, TA29, and TA32 anti-mRNA probes produced identical, tapetal-specific localization patterns, as did TA13 and TA36 anti-mRNA probes (data not shown). For example, the TA29 anti-mRNA probe produced an intense hybridization signal over the tapetum at stage 3 (Figure 5H) and did not produce any hybridization grains above background over any other

anther regions. Nor were there any detectable hybridization signals produced at stage 1 (Figure 5G) and stage 6 (Figure 5I). The hybridization signals at each stage correlated directly with the mRNA levels observed in the RNA dot blot and gel blot experiments (Figures 4A and 4C). The absence of a detectable signal at stage 6 (Figures 5F, 5I, and 5L) coincided with the degeneration process occurring in the tapetum (Figure 2 and Table 1).

We hybridized ^{3}H-poly(U) with the anther sections to localize the distribution of total poly(A) RNA molecules. In contrast with the results obtained with the TA13, TA26, TA29, TA32, and TA36 anti-mRNA probes (Figure 5), the distribution of grains was uniform throughout the anther at each stage investigated and grains were present over all tissues (data not shown). Together, these results indicate that several different mRNAs that accumulate and decay coordinately during early phase 2 of anther development are localized within the tapetum and that these mRNAs include those encoding the glycine-rich proteins (TA13, TA29) and the lipid transfer proteins (TA32, TA36).

The TA56 Thiol Endopeptidase mRNA Is Localized within the Connective and Stomium

The TA56 mRNA localization pattern is shown in Figure 6. Figures 6A to 6D show that the TA56 mRNA control probe produced no hybridization grains above background levels with anther sections from stage 1 (Figure 6A), stage 3 (Figure 6B), stage 8 (Figure 6C), and stage 11 (Figure 6D). By contrast, Figures 6E to 6H show that the TA56 anti-mRNA probe produced a localized hybridization signal at all stages investigated and that both the location and intensity of the hybridization grains changed with the developmental state of the anther. Bright-field photographs of the anther regions containing the TA56 mRNA are shown in Figures 6I to 6L, and Figures 6M to 6P show high-magnification dark-field photographs of the hybridization grains at each stage.

As predicted from the RNA accumulation studies (Figures 4B and 4C), a relatively weak TA56 hybridization signal was observed at stage 1 of anther development (Figures 6E and 6M). This signal was localized on both sides of the anther over a circular cluster of cells between the stomium and the connective (Figures 6E, 6I, and 6M). At stage 3, the TA56 mRNA hybridization signal intensified

Figure 2. (continued).

epidermis; En, endothecium; MMC, microspore mother cells; Msp, microspores; PS, pollen sac; S, stomium; Sp, sporogenous cells; T, tapetum; TDS, tetrads; V, vascular bundle. Magnification factors for stage −7, −6, −2, 1, 3, and 8 anthers were ×400, ×200, ×100, ×100, ×100, and ×100, respectively.

(A) Anther development in wild-type untransformed plants.

(B) Anther development in plants transformed with a chimeric TA29/DTA gene. Tobacco plants were transformed with a TA29/DTA gene as described in Methods. The TA29/DTA gene contained a TA29 5′ DNA fragment containing nucleotides −1477 to +51 (Mariani et al., 1990; Seurinck et al., 1990) fused with the DTA gene coding sequence (Greenfield et al., 1983; Maxwell et al., 1986; Palmiter et al., 1987).
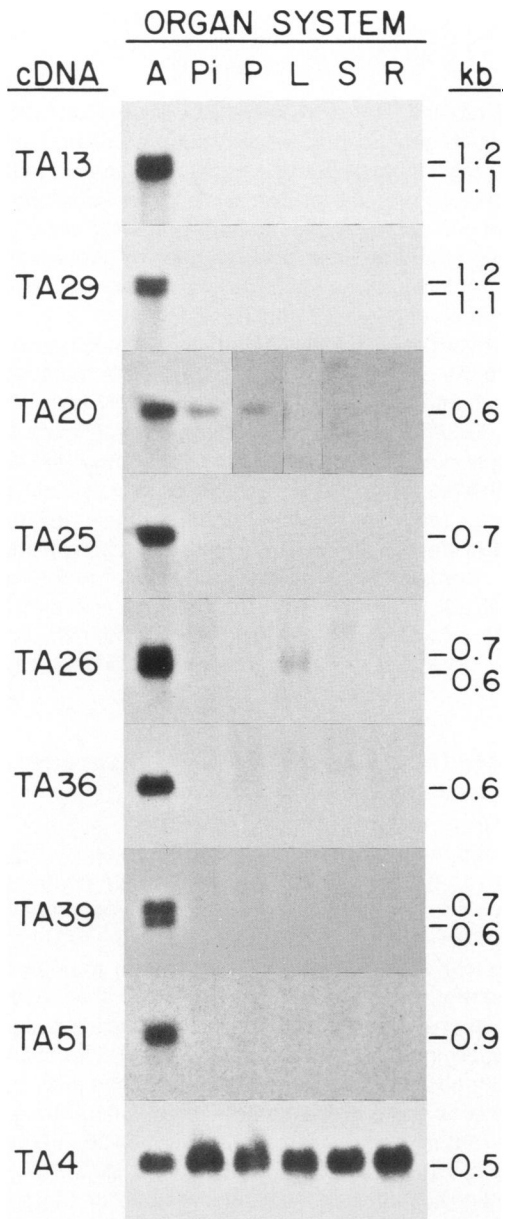
Figure 3. Representation of Anther-Specific mRNAs in Floral and Vegetative Organ Systems.

Tobacco anther (A), pistil (Pi), petal (P), leaf (L), stem (S), and root (R) polysomal poly(A) mRNAs were fractionated on denaturing agarose gels, transferred to nitrocellulose paper, and hybridized with labeled plasmid DNA probes as outlined in Methods. Anther and pistil mRNAs were isolated from stage 6 flower buds (Figure 1), whereas petal mRNA was isolated from stage 12 flowers (Figure 1). Leaf, stem, and root mRNAs were isolated from plants described in Methods. One microgram of each mRNA was used for the TA29 gel blot, and 0.5 μg of each mRNA was used for the TA13, TA20, and TA25 gel blots. By contrast, the TA26, TA35, TA51, and TA4 gel blots contained 0.1 μg of anther mRNA and 1 μg of all other mRNAs. Film exposure times varied for each gel blot but, with the exception of the TA20 gel blot, were the same for all RNA lanes. Exposure times for the TA20 petal, leaf, stem, and root RNA lanes were approximately 30 times longer than that used for the anther and pistil RNA lanes.

but remained localized over the same circular cell cluster (Figures 6F, 6J, and 6N). No hybridization grains above background levels were observed over any other anther tissues at this stage, including the epidermis, connective, endothecium, tapetum, and wall. By stage 8, however, the TA56 mRNA localization pattern changed. Figures 6G, 6K, and 6O show that the TA56 mRNA was now localized over both stomium regions and was uniformly distributed over the connective separating the pollen sacs. By contrast, TA56 mRNA was undetectable in the circular cell cluster between the stomium and connective because these cells had degenerated (Figure 6K). Finally, at stage 11 after the connective degenerated (Table 1), the TA56 mRNA hybridization signal was reduced significantly but was still localized over the stomial cells (Figures 6H, 6L, and 6P). Together, these data indicate that the TA56 thiol endopeptidase mRNA is present in specific anther cell types and that the appearance of this mRNA occurs just before the degeneration of these cells in anther development.

The TA20 mRNA Is Distributed throughout the Anther and Is Localized in Specific Pistil Regions

Figures 3 and 4B show that the TA20 mRNA is present throughout phase 2 of anther development and is also present in the pistil at a level 10-fold lower than that observed in anthers of the same stage flower bud. We hybridized a TA20 anti-mRNA probe with anther and pistil sections to localize TA20 molecules within both of these floral organ systems. Figure 7A shows that this probe produced an intense hybridization signal over most anther tissues at stage 2, including the connective, stomium, and wall layers. Highest concentrations of grains occurred over the connective and over cells immediately surrounding the tapetum. By contrast, the TA20 anti-mRNA probe did not produce any hybridization grains above background levels (Figure 7E) over the vascular bundle, the tapetum, or the circular cell cluster between the stomium and connective that contained the TA56 thiol endopeptidase mRNA (Figures 6M and 6N). Figures 7B to 7D show that at later developmental stages the TA20 mRNA remained localized within the same tissues, but beginning at stage 6 became progressively concentrated in connective regions adjacent to the vascular bundle (Figure 7C), and by stage 8 became less prevalent throughout the anther (Figure 7D).

Figures 8A to 8C show bright-field photographs of ovary cross-sections from a stage 4 pistil (Figure 8A) and a stage 6 pistil (Figure 8B), as well as a stigma/style longitudinal section from a pistil at stage 6 (Figure 8C). Two carpels can be visualized within the ovary of each pistil, along with locules, placenta, vascular bundle, ovules, and the ovary wall (Figures 8A and 8B). A prominent stigma and a style with transmitting tissue were also visualized within the pistil (Figure 8C). Figures 8D and 8E show that the TA20 mRNA was localized within the ovary wall and a narrow cell layer that connects the ovules to the placenta. No TA20 hybridization grains above background levels (data
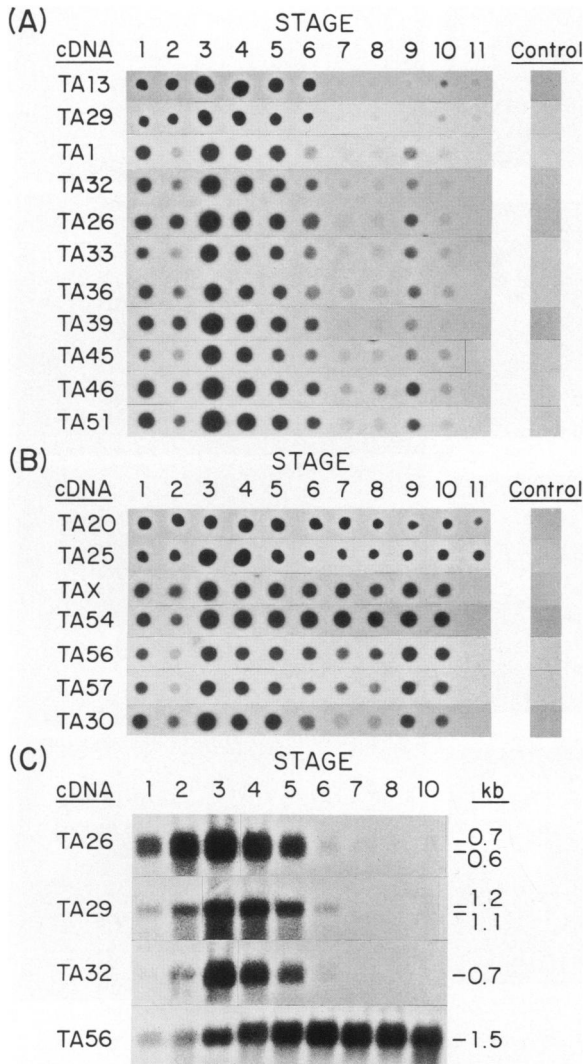
Figure 4. Accumulation of Anther-Specific mRNAs during Anther Development.

Polysomal poly(A) mRNAs were isolated from anthers at different developmental stages (Figure 1) and either spotted onto nitrocellulose paper [(A) and (B)] or fractionated on denaturing agarose gels and transferred to nytran [(C)]. Dot blots and gel blots were hybridized with labeled plasmid DNAs as outlined in Methods. Film exposure times differed for each dot blot or gel blot developmental series but were the same for each RNA hybridized with a given DNA probe.

(A) Hybridization of anther cDNA plasmids with anther mRNAs at different developmental stages. The TA13 and TA29 dots contained 0.25 μg of mRNA; the other dots contained 0.05 μg of mRNA. Control dots contained an equivalent amount of soybean embryo polysomal poly(A) mRNA.

(B) Hybridization of anther cDNA plasmids with anther mRNAs at different developmental stages. The TA20 and TA25 dots contained 0.25 μg of mRNA; the other dots contained 0.05 μg of mRNA. Control dots contained an equivalent amount of soybean embryo polysomal poly(A) mRNA.

not shown) were observed over the ovules, vascular bundles, and most of the placenta. Figure 8F shows that TA20 hybridization grains were also absent from the stigma and the transmitting tissue of the style. By contrast, TA20 mRNA molecules were localized within parenchyma tissue that extended from beneath the stigma surface through the style to the ovary (Figure 8F). Together, these data show that the TA20 mRNA is present in the majority of anther cells throughout phase 2 of development and is concentrated within specific regions of the pistil. We conclude from these data and those obtained with the other mRNAs (Figures 5 and 6) that temporal differences in anther gene expression programs correlate with the differentiation and degeneration of specific anther cell types.

Most Anther Genes Are Represented only a Few Times in the Tobacco Genome

We hybridized stage 6 anther ^{32}P-cDNA with an excess of tobacco DNA in solution to estimate the copy number of genes expressed in the anther. We utilized an internal ^{3}H-single-copy DNA standard to calibrate the hybridization kinetics (Goldberg et al., 1978, 1981). Figure 9A shows that 70% of the ^{32}P-cDNA hybridized with a rate constant identical to that of the ^{3}H-single-copy DNA (0.00045 M^{-1} sec^{-1}). By contrast, 30% of the ^{32}P-cDNA hybridized with a rate constant of 0.047 M^{-1} sec^{-1}, suggesting that these sequences are reiterated approximately 100 times (0.047/0.0045) in the tobacco genome. These studies, and those presented previously (Kamalay and Goldberg, 1980), indicate that mRNAs comprising most of the stage 6 anther mRNA mass and sequence complexity are encoded by single-copy genes, or genes present only a few times (<5) per tobacco genome.

We hybridized anther cDNA plasmids with DNA gel blots to estimate the copy number of individual anther-specific genes. We utilized several tapetal-specific cDNA plasmids for these experiments (Figure 5) and included those representing the glycine-rich protein mRNAs (TA29, TA13) and the lipid transfer protein mRNAs (TA32, TA36) (Table 2). Figure 9B shows that each of these probes hybridized with only three or four EcoRI fragments in the tobacco genome at the hybridization criterion employed (42°C, 50% formamide, 1 M Na$^+$). For example, the TA29 plasmid probe hybridized with two similar-sized EcoRI fragments 6.5 kb to 7.0 kb in length and two additional EcoRI fragments 8.6 kb and 10.5 kb in length, respectively. The restriction map of the TA29 gene region, shown in Figure 10A, and sequencing studies with TA13 and TA29 cDNAs (Seurinck et al., 1990; J. Seurinck, J. Leemans, and R.B.

(C) Hybridization of the TA26, TA29, TA32, and TA56 cDNA plasmids with anther mRNAs at different developmental stages. Each RNA gel blot contained 0.7 μg of mRNA per lane. The TA26, TA29, TA32, and TA56 RNA gel blots were exposed for 1.5 hr, 1.5 hr, 5 hr, and 96 hr, respectively.
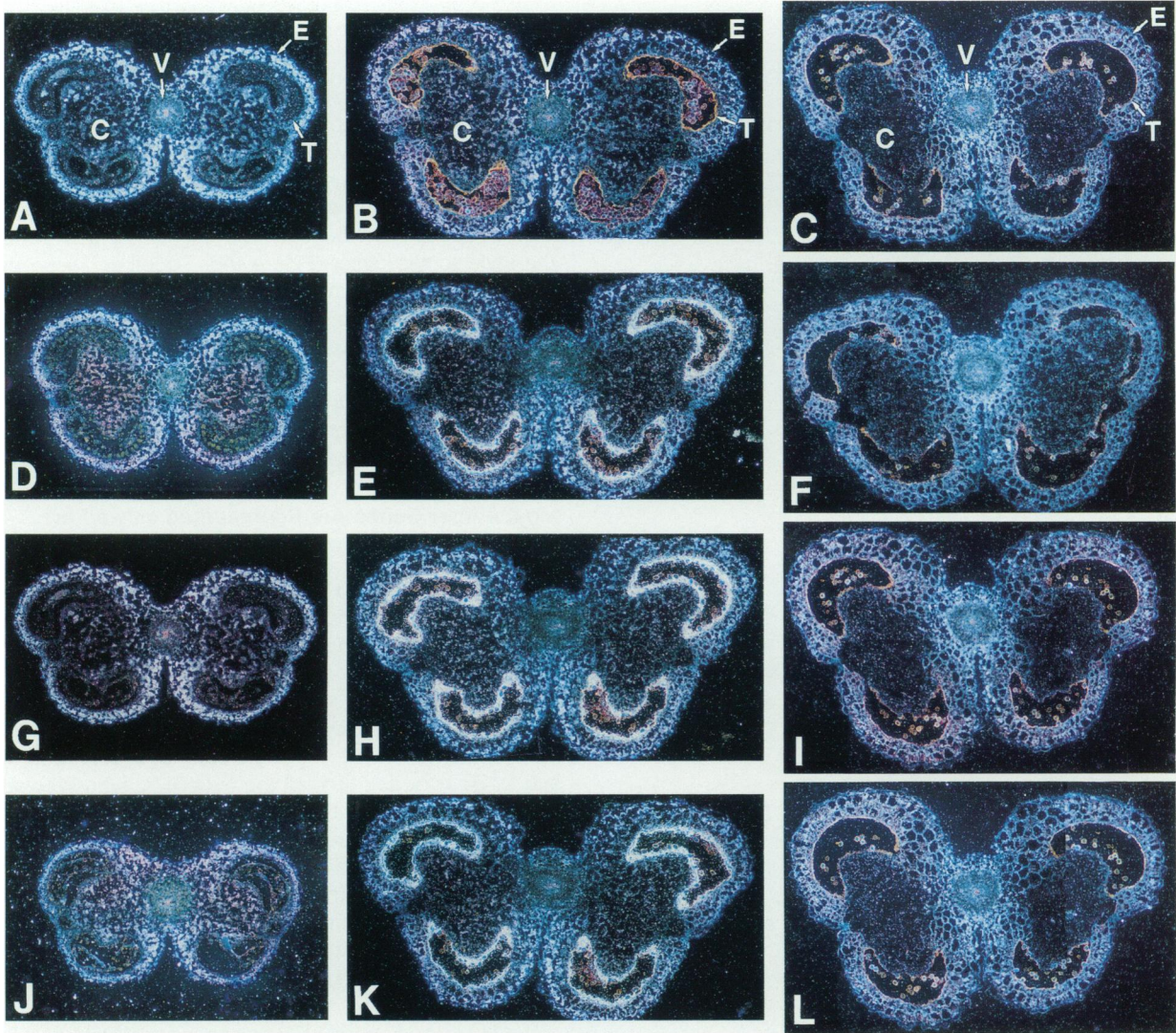
Figure 5. Localization of the TA26, TA29, and TA32 mRNAs during Tobacco Anther Development.

Anthers were fixed, embedded in paraffin, sliced into 10-μm sections, and hybridized with single-stranded ^{35}S-RNA probes as outlined in Methods. Photographs were taken by dark-field microscopy, and all film emulsion exposures were for 3.5 days. Corresponding bright-field photographs are shown in Figure 2. Magnification factors for the stage 1, stage 3, and stage 6 anthers were ×100, ×100, and ×66, respectively. C, connective; E, epidermis; T, tapetum; V, vascular bundle.

(A) to **(C)** In situ hybridization of a TA29 mRNA control probe with anthers at stage 1 [**(A)**], stage 3 [**(B)**], and stage 6 [**(C)**]. White grains represent background hybridization levels; white patchy areas in the anther wall represent light-scattering effects due to dark-field illumination through stained sections.

(D) to **(F)** In situ hybridization of a TA26 anti-mRNA probe with anthers at stage 1 [**(D)**], stage 3 [**(E)**], and stage 6 [**(F)**]. White grains in the stage 3 anther represent regions containing RNA/RNA hybrids.

(G) to **(I)** In situ hybridization of a TA29 anti-mRNA probe with anthers at stage 1 [**(G)**], stage 3 [**(H)**], and stage 6 [**(I)**]. White grains in the stage 3 anther represent regions containing RNA/RNA hybrids.

(J) to **(L)** In situ hybridization of a TA32 anti-mRNA probe with anthers at stage 1 [**(J)**], stage 3 [**(K)**], and stage 6 [**(L)**]. White grains in the stage 3 anther represent regions containing RNA/RNA hybrids.

Goldberg, unpublished data) indicated that these EcoRI fragments were derived from cleavage of the TA13 and TA29 genes. DNA sequencing studies (J. Seurinck, J. Leemans, and R.B. Goldberg, unpublished results) also suggested that each TA32 and TA36 EcoRI fragment

represented a different gene (Figure 9B). Together, these data indicate that each tapetal-specific mRNA investigated is encoded by a small gene family.

We hybridized the TA29 cDNA plasmid with gel blots containing tobacco DNA (*Nicotiana tabacum*) and the
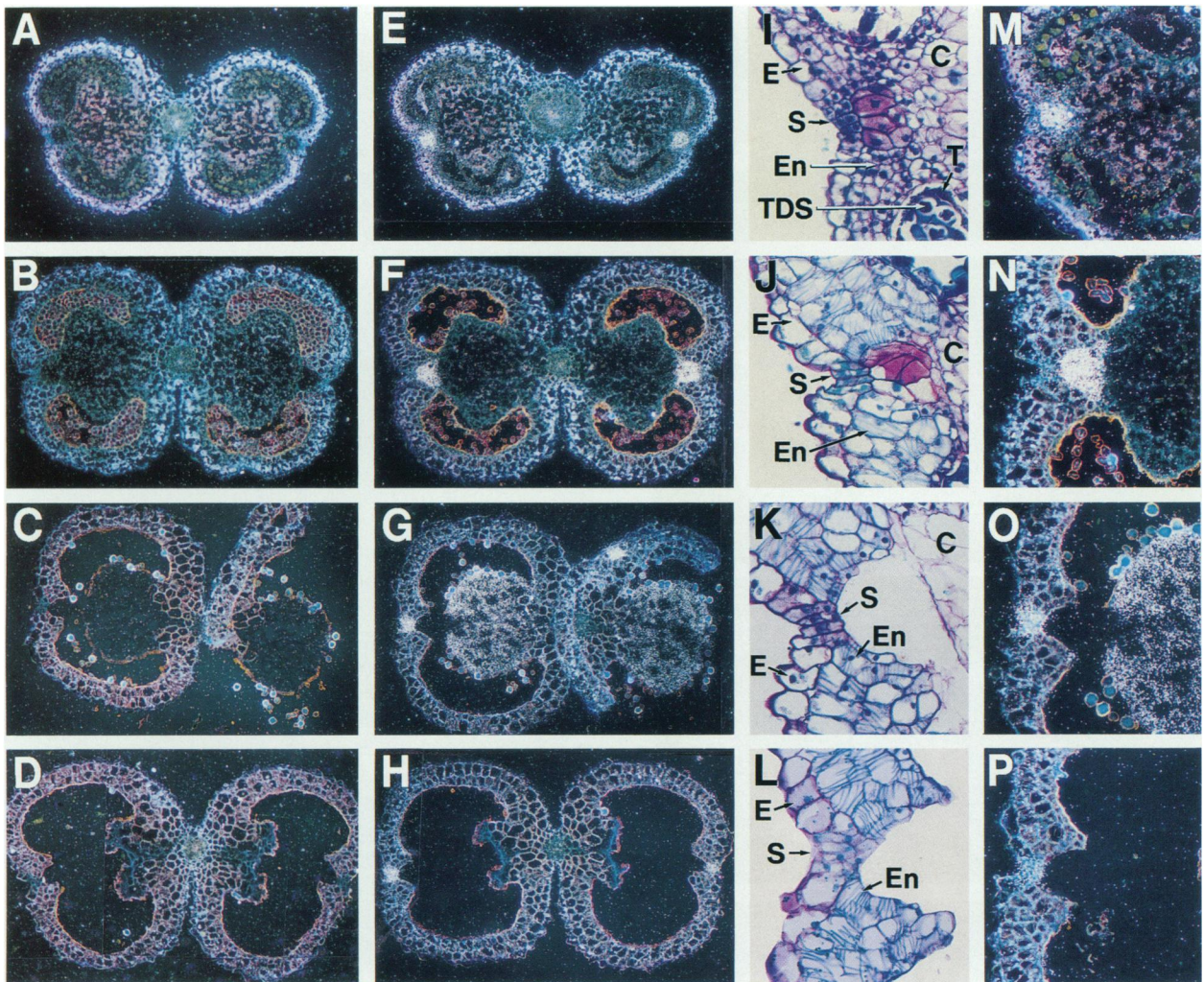
Figure 6. Localization of the TA56 mRNA during Tobacco Anther Development.

Anthers were fixed, embedded in paraffin, sliced into 10-μm sections, and hybridized with single-stranded ^{35}S-RNA probes as outlined in Methods. C, connective; E, epidermis; En, endothecium; S, stomium; T, tapetum; TDS, tetrads.

(A) to **(D)** In situ hybridization of a TA56 mRNA control probe with anthers at stage 1 [**(A)**], stage 3 [**(B)**], stage 8 [**(C)**], and stage 11 [**(D)**]. Photographs taken with dark-field microscopy, and film emulsion exposure times were for 13 days. White grains represent background hybridization levels; white patchy areas represent light-scattering effects due to dark-field illumination through stained anther sections. The magnification factor for anthers at each stage was ×100.

**(E)** to **(H)** In situ hybridization of a TA56 anti-mRNA probe with anther sections at stage 1 [**(E)**], stage 3 [**(F)**], stage 8 [**(G)**], and stage 11 [**(H)**]. Photographs were taken with dark-field microscopy, and film emulsion exposure times were for 13 days. White grains represent regions containing RNA/RNA hybrids. The magnification factor for anthers at each stage was ×100.

(I) to **(L)** Bright-field photographs of anther stomium region at stage 1 [**(I)**], stage 3 [**(J)**], stage 8 [**(K)**], and stage 11 [**(L)**]. Anther regions correspond to those showing intense hybridization in **(E)** through **(H)** and **(M)** through **(P)**. The magnification factor for anthers at each stage was ×400.

(M) to **(P)** In situ hybridization of a TA56 anti-mRNA probe with anther stomium region at stage 1 [**(M)**], stage 3 [**(N)**], stage 8 [**(O)**], and stage 11 [**(P)**]. Dark-field photographs represent the stomium region of anthers shown in **(E)** to **(H)** at a magnification factor of ×350.

DNAs of its diploid progenitor species (*N. tomentosiformis* and *N. sylvestris*; Goodspeed, 1954) to determine whether genes encoding this tapetal-specific mRNA were derived from one or both tobacco parental lines. As seen in Figure 9C, the gel blot hybridization patterns obtained with all three tobacco DNAs were similar with the exception of
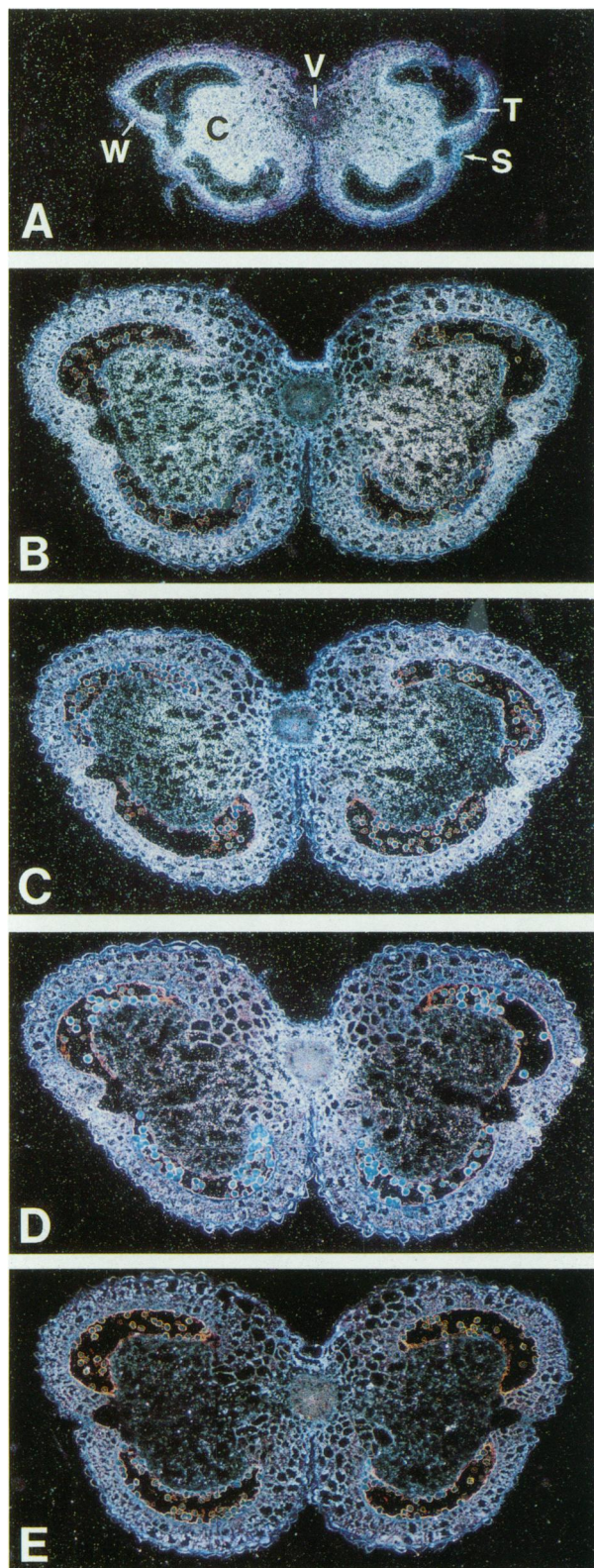
one or two polymorphisms. Polymorphic DNA fragments were not unexpected because our previous experiments showed that *N. tomentosiformis* and *N. sylvestris* single-copy DNAs had diverged considerably from each other (Okamuro and Goldberg, 1985). Together, these results indicate that members of the TA13/TA29 glycine-rich protein gene family are present in both parental species of *N. tabacum* and that these genes were probably present in the genus before the divergence of *N. sylvestris* and *N. tomentosiformis* from a common ancestor (Goodspeed, 1954).

The TA29 Gene Does not Contain Introns and Is Contiguous to a Constitutively Expressed Gene

We isolated a genomic clone containing the TA29 gene (Figure 10A) to begin to dissect processes that regulate the coordinate expression of the tapetal-specific gene set (Figures 3 to 5). We hybridized λTA29 phage DNA with anther mRNA under conditions that form R-loops to visualize TA29 gene structure in the electron microscope (see Methods). Figure 10A shows that the TA29 R-loops were simple in structure and lacked detectable introns, and that their average length was approximately the size of the TA29 mRNAs. The TA29 gene sequence confirmed the absence of introns and revealed that this gene has a continuous open reading frame of 963 bp (Seurinck et al., 1990). Translation of the reading frame indicated that the TA29 gene encoded a 33-kD glycine-rich protein that has several potential glycosylation sites and is organized into two similar 120-amino acid modules that are highly hydrophobic (Seurinck et al., 1990). A schematic representation of the TA29 gene, including the positions of relevant consensus sequences, is shown in Figure 10A.

We hybridized the λTA29 phage DNA with gel blots containing floral and vegetative organ system mRNAs to determine whether other genes were present in the TA29 gene region. Figure 10B shows that the phage probe produced an intense hybridization signal with the 1.1-kb and 1.2-kb TA29 anther mRNAs. In addition, this probe

Figure 7. Localization of the TA20 mRNA during Tobacco Anther Development.

Anthers were fixed, embedded in paraffin, sliced into 10-μm sections, and hybridized with single-stranded ^{35}S-RNA probes as outlined in Methods. Photographs were taken by dark-field microscopy, film emulsion exposure times were 6 days, and the magnification factor for anthers at each stage was ×100. Corresponding bright-field photographs are shown in Figure 2. C, connective; S, stomium; T, tapetum; V, vascular bundle; W, wall. **(A)** to **(D)** In situ hybridization of a TA20 anti-mRNA probe with anthers at stage 2 [**(A)**], stage 4 [**(B)**], stage 6 [**(C)**], and stage 8 [**(D)**]. White grains represent regions of RNA/RNA hybridization. **(E)** In situ hybridization of a TA20 mRNA control probe with a stage 4 anther. White grains represent background hybridization levels.
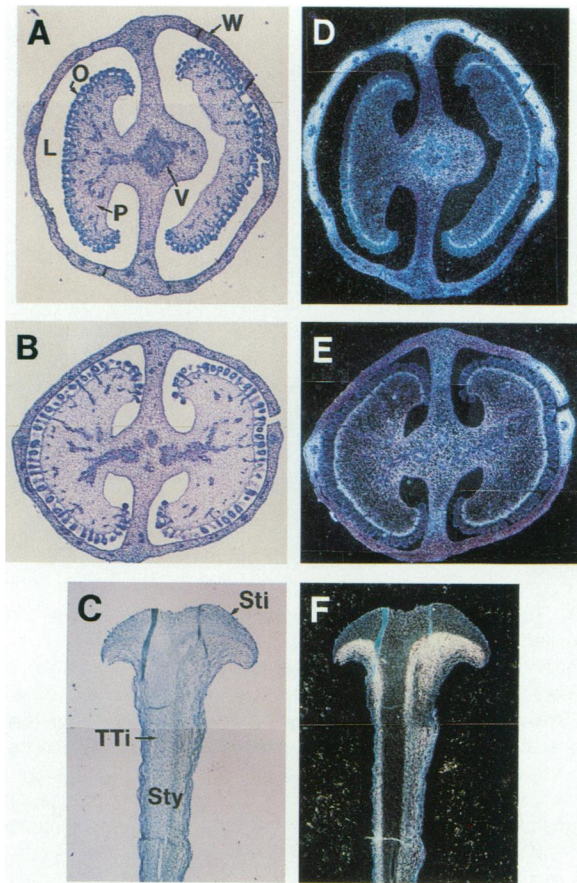
Figure 8. Localization of the TA20 mRNA within the Tobacco Pistil.

Pistils were fixed, embedded in paraffin, sliced into 10-μm sections, and hybridized with a TA20 anti-mRNA probe as outlined in Methods. The film emulsion exposure times and magnification factors were 6 days and ×40, respectively. L, locule; O, ovule; P, placenta; TTi, transmitting tissue; Sti, stigma; Sty, style; V, vascular bundle; W, wall.

(A) and **(B)** Bright-field photographs of ovary cross-sections from pistils at stage 4 [**(A)**] and stage 6 [**(B)**].

(C) Bright-field photograph of a stigma and style longitudinal section from a stage 6 pistil.

(D) and **(E)** In situ hybridization of a TA20 anti-mRNA probe with ovaries from pistils at stage 4 [**(D)**] and stage 6 [**(E)**]. Photographs were taken by dark-field microscopy. White grains represent regions of RNA/RNA hybridization.

(F) In situ hybridization of a TA20 anti-mRNA probe with the stigma and style of a stage 6 pistil. Photograph was taken by dark-field microscopy. White grains represent regions of RNA/RNA hybridization.

hybridized weakly with a 0.9-kb mRNA in all other organs. The prevalence of the 0.9-kb mRNA in the leaf, root, pistil, and petal was at least 2 orders of magnitude lower than

that observed for the TA29 anther mRNAs. By contrast, the 0.9-kb mRNA was approximately 10-fold more prevalent in the stem than in the other organs (Figure 10B).

We localized DNA sequences responsible for producing the 0.9-kb mRNA signal to a region just 3′ to the TA29 gene (Figure 10A). R-loop studies with stem mRNA (Figure 10A) and the DNA sequence of this region (Seurinck et al., 1990) revealed the presence of a gene with two introns that was transcribed in the opposite direction as the TA29 gene. We designated this gene as TSJT1 (Seurinck et al., 1990), and a schematic representation of its structure and position in the TA29 gene region is shown in Figure 10A. The TSJT1 coding sequence was not related to any known gene or protein in the GenBank.

We hybridized a DNA fragment containing a portion of the TSJT1 gene with gel blots containing floral and vegetative organ system mRNAs to determine whether it was also active in the anther. Figure 10C shows that a 0.9-kb TSJT1 mRNA signal was produced with anther mRNA at a level equivalent to that observed with all organ system mRNAs except the stem. Together, these data show that the TA29 tapetal-specific gene has a relatively simple structure and that it is contiguous to a convergently transcribed gene that is differentially regulated and expressed in all organ systems.

The TA29 Gene Is Regulated at the Transcriptional Level

We hybridized DNA gel blots containing TA29 gene sequences with ^{32}P-RNAs synthesized in isolated anther and leaf nuclei (see Methods) to determine whether the organ specificity of the TA29 gene was controlled by transcriptional or post-transcriptional processes. We included TSJT1 DNA sequences on these blots as a control because this gene was active in both the anther and the leaf (Figure 10C). The results are shown in Figures 11A and 11B and are summarized schematically in Figure 11C.

Figure 11 shows that both the TA29 gene (Figure 11A) and the TSJT1 gene (Figure 11B) hybridized with anther ^{32}P-nuclear RNA. The TSJT1 hybridization signal was slightly more intense than that obtained with the TA29 gene, even though the 0.9-kb TSJT1 mRNA was approximately 100-fold less prevalent than the TA29 mRNAs in the anther (Figures 10B and 10C). By contrast, no detectable TA29 gene hybridization signal was observed with leaf ^{32}P-nuclear RNA (Figure 11A), even though this probe produced a signal with DNA fragments representing the TSJT1 gene (Figure 11B). Together, these data indicate that the TA29 gene is regulated primarily at the transcriptional level and that post-transcriptional processes contribute to establishing TA29 and TSJT1 mRNA levels in the anther.
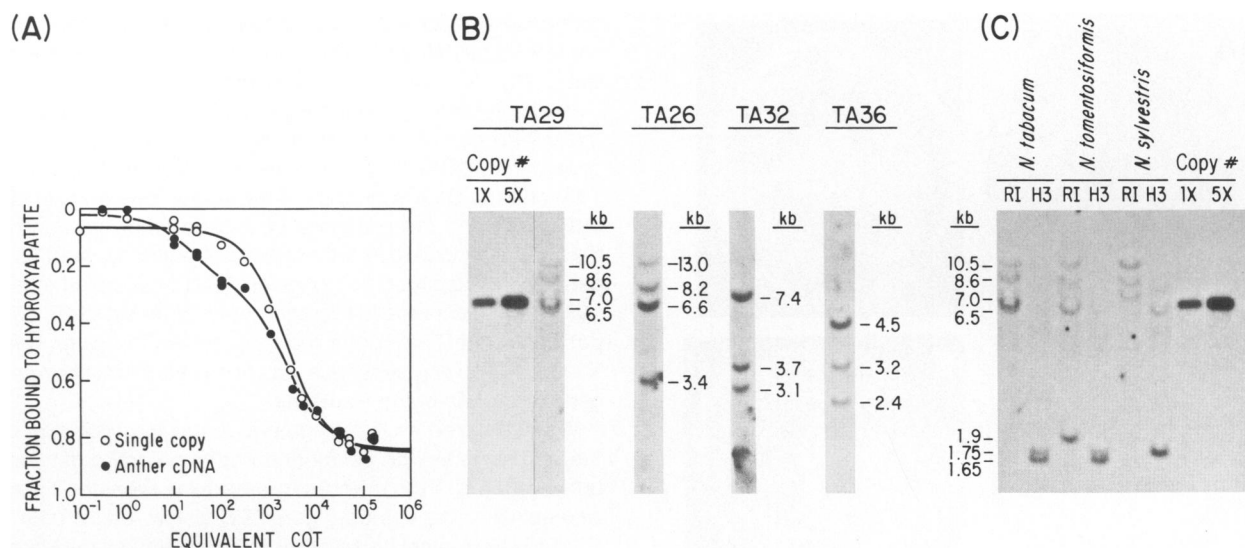
Figure 9. Representation of Anther mRNA Sequences in the Tobacco Genome.

(A) Hybridization of stage 6 anther cDNA with an excess of tobacco DNA. Trace amounts of ^{32}P-anther cDNA and ^{3}H-single-copy DNA were hybridized together with an excess (>25,000/1 mass ratio) of unlabeled total genomic DNA, and the extent of hybridization was measured by hydroxyapatite chromatography (see Methods). The single-stranded fragment size of driver and tracer DNAs was 0.3 kb. The reassociation kinetics of the driver genomic DNA were described elsewhere (Zimmerman and Goldberg, 1977; Okamuro and Goldberg, 1985). Curves through the data points represent the best least-squares solution for either one second-order component (single-copy DNA) or two second-order components (anther cDNA). For these solutions, the rate constant of the slowest hybridizing (single-copy) component was fixed at 0.00045 M^{-1} sec^{-1}, a value obtained previously from several independent reassociation experiments with tobacco single-copy DNA (Goldberg et al., 1978; Kamalay and Goldberg, 1980; Okamuro and Goldberg, 1985). Other solutions to these data points produced higher root mean square errors. The fraction of DNA fragments, second-order rate constant, and average copy number for each component were: ^{3}H-cDNA; component 1, 0.29, 0.047 M^{-1} sec^{-1}, 100; component 2, 0.71, 0.00045 M^{-1} sec^{-1}, 1; ^{32}P-single-copy DNA; component 1, 1.0, 0.00045 M^{-1} sec^{-1}, 1. The fraction of DNA fragments in each component was normalized to 100% tracer reactivity (Kamalay and Goldberg, 1980; Okamuro and Goldberg, 1985).

(B) Hybridization of tobacco DNA gel blots with labeled TA26, TA29, TA32, and TA36 plasmid DNAs. Tobacco DNA was digested with EcoRI, fractionated by electrophoresis on agarose gels, transferred to nitrocellulose, and hybridized with each labeled plasmid DNA as outlined in Methods. The reconstruction lanes contained one copy (1×) and five copy (5×) equivalents of EcoRI-digested λTA29 phage DNA (Figure 10) and were calculated using a λTA29 phage DNA length of 43 kb (Figure 10) and an *N. tabacum* genome size of 2.4 × 10^6 kb [(A) and Okamuro and Goldberg, 1985]. The TA29 probe hybridized with TA13 sequences at the criterion employed, whereas the TA32 and TA36 probes did not hybridize significantly to each other (Table 2).

(C) Hybridization of labeled TA29 plasmid DNA with gel blots containing DNAs of different tobacco species. Tobacco DNAs were digested with the designated restriction endonucleases, fractionated by electrophoresis on agarose gels, and hybridized with labeled TA29 plasmid DNA as described in Methods. The one copy (1×) and five copy (5×) reconstruction lanes were calculated on the basis of the *N. tabacum* genome size as described in **(B)**.

A 122-bp 5′ Region Programs TA29 Gene Tapetal-Specific Expression

We showed elsewhere (Mariani et al., 1990) that the TA29 gene 5′ region can direct *Escherichia coli* β-glucuronidase (GUS) gene expression within the tapetum, and that the chimeric TA29/GUS gene is regulated exactly like the endogenous TA29 gene (Figures 3 to 5). We generated deletions of the TA29 gene 5′ region to localize sequences required to activate TA29 gene transcription within tapetal cells. These deletions were fused with the GUS gene and then the chimeric TA29/GUS genes were transferred to tobacco plants (see Methods). A schematic representation of some of the chimeric TA29/GUS genes is shown in Figure 12A. We obtained 170 transformants representing 20 different 5′ deletions ranging from −5670 to +18 nucleotides relative to the TA29 transcription start site (Figures 10A and 12A). The number of individual transformants per deletion varied from one (−2070) to 19 (−1990), but averaged approximately nine. DNA gel blot studies and genetic analysis of kanamycin-resistant (Kn^r) gene segregation patterns showed that most transformants had one unrearranged copy of the TA29/GUS gene (data not shown).
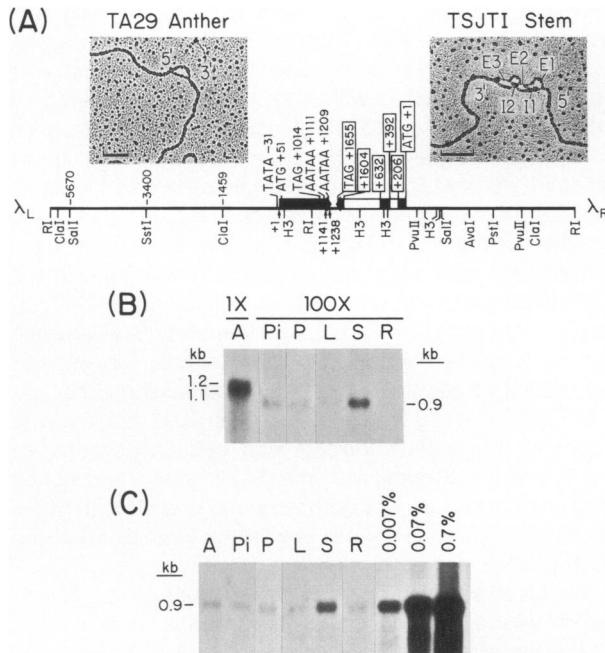
Figure 10. Organization of the TA29 Anther Gene Region.

(A) Structures of the TA29 anther gene and contiguous TSJT1 stem gene. The TA29 cDNA plasmid was used to isolate a 13.2-kb genomic clone from an EcoRI λCharon 32 tobacco DNA library (Seurinck et al., 1990). DNA gel blot experiments (Figures 9B and 9C) showed that this clone represents an unrearranged copy of the TA29 genomic region. The 6.2-kb ClaI/AvaI region containing the anther and stem genes was sequenced by Seurinck et al. (1990). Large arrows represent gene locations and transcriptional orientations. Solid and open regions represent exons and introns, respectively. TA29 nucleotides +1, +1141, and +1238 indicate the transcription start site and 3′ gene ends as determined by both S1 nuclease and primer extension analyses. The TA29 cDNA plasmid represents nucleotides +452 to +821. The TSJT1 stem gene is numbered relative to the ATG start codon because the transcription start site has not yet been determined. Nucleotide coordinates for each exon, as well as the start and stop codons, are boxed. Fusion of the three stem gene exons results in an open reading frame of 498 nucleotides, which is approximately 60% of the mRNA length [**(B)** and **(C)**]. The TA29 gene 3′ end is only 412 nucleotides from the TSJT1 gene stop codon (Seurinck et al., 1990). Only relevant λTA29 restriction endonuclease sites are shown. Sites contained within the 6.2-kb ClaI/AvaI region can be obtained from the DNA sequence (Seurinck et al., 1990). λ_L and λ_R refer to the λCharon 32 left and right arms, respectively. The R-loops were formed by hybridizing a sequence excess of either anther mRNA or stem mRNA with λTA29 DNA as described by Fischer and Goldberg (1982). The bar in the electron micrographs represents 1 kb. E and I refer to exons and introns, respectively. The number-average anther gene R-loop size was 0.84 ± 0.2 kb (n = 26). The R-loop and intron sizes for the stem gene were: 0.31 kb (E1), 0.22 kb (I1), 0.29 kb (E2), 0.42 kb (I2), and 0.35 kb (E3) (n = 1). The anther and stem gene R-loops were oriented relative to the λTA29 restriction endonuclease map and the λCharon 32 left and right arms.

(B) Representation of λTA29 sequences in vegetative and floral

We used fluorimetric analysis to measure GUS enzyme activity in stage 4 anthers from 148 individual transformants. Although the GUS enzyme levels varied between transformants with a given deletion, the results showed that TA29/GUS gene transcriptional activity remained relatively constant as the 5′ region was deleted from −5670 to −279 nucleotides (data not shown). By contrast, no detectable GUS enzyme activity was observed in anthers containing TA29/GUS genes with only 150 nucleotides of TA29 5′ region (data not shown). We hybridized a GUS probe with gel blots containing pooled stage 4 anther mRNAs from five independent transformants per deletion (Figure 12A) to show directly that transcriptional control sequences were localized between −279 and −150 nucleotides from the TA29 gene transcriptional start site (Figures 10A and 12A). Figure 12B shows that GUS mRNA levels were similar in transformants containing TA29/GUS genes with 5270 to 279 nucleotides of the TA29 5′ region. Relative to the RNA standards shown in Figure 12C, the GUS mRNA prevalence in these transformants averaged 0.1%, a value similar to that obtained for the endogenous TA29 mRNA gene at the same developmental stage (Table 2). In situ hybridization studies showed directly that tapetal cell GUS and TA29 mRNA levels were similar in TA29/GUS transformants containing either 5270 or 1477 nucleotides of the TA29 5′ region (Mariani et al., 1990; K.H. Cox and R.B. Goldberg, unpublished results). By contrast, no detectable GUS mRNA was observed in transformants containing either 150 nucleotides of the TA29 5′ region or no TA29 5′ region, even though endogenous TA26 mRNA levels were similar to those obtained in all of the other transformants (Figure 12B). This result indicated that the TA29/GUS gene transcriptional level dropped to below our detection limit (>100-fold) when the TA29 5′ region was deleted from −279 to −150 nucleotides. Together, these

organ system mRNAs. Anther (A), pistil (Pi), petal (P), leaf (L), stem (S), and root (R) mRNAs were fractionated by electrophoresis on denaturing agarose gels, transferred to nitrocellulose, and hybridized with labeled λTA29 phage DNA as outlined in Methods. Anther and pistil mRNAs were isolated from stage 6 flowers; petal mRNA was isolated from stage 12 flowers (Figure 1). Each lane contained 0.5 μg of mRNA, but the anther mRNA gel blot (1×) was exposed for only 1/100 of the time used to expose the other gel blots (100×).

(C) Representation of the TSJT1 gene sequence in vegetative and floral organ system mRNAs. Gel blot conditions and mRNAs were the same as those used in **(B)**. For these gel blots, a DNA fragment containing portions of the TSJT1 stem gene exon 2 and intron 2 [0.7-kb HindIII fragment, **(A)**] was used as a probe. The reconstruction lanes contained 0.5 μg (0.7%), 0.05 μg (0.07%), and 0.005 μg (0.007%) of soybean midmaturation stage mRNA, and were hybridized with the soybean L9 lectin cDNA plasmid (Goldberg et al., 1983). Experiments published previously established that the 1-kb lectin mRNA represents approximately 0.7% of the midmaturation stage embryo mRNA (Goldberg et al., 1983). All gel blot RNA lanes were exposed for 3 days.
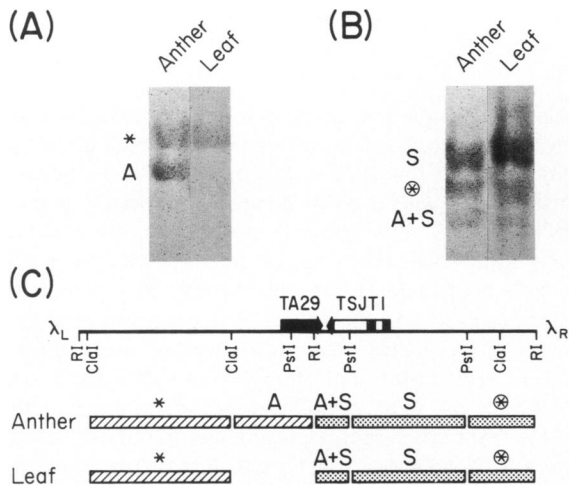
Figure 11. Transcriptional Regulation of the Tapetal-Specific TA29 Gene.

(A) Hybridization of the TA29 gene with anther and leaf ^{32}P-nuclear RNAs. A plasmid (TA29Eco6.6L) representing the left half of the λTA29 phage DNA (Figure 10A) was digested with both ClaI and EcoRI, transferred to nytran, and hybridized with ^{32}P-nuclear RNAs synthesized in vitro from either stage 3 anther nuclei or leaf nuclei (see Methods). The band labeled with an asterisk represents an RNA polymerase II (α-amanatin sensitive) transcript that hybridized with the 4.2-kb ClaI DNA fragment [(C)]. An RNA complementary to DNA sequences in this region was not detected in the gel blot experiments with organ system mRNAs shown in Figure 10B. The band labeled A represents the TA29 nuclear RNA that hybridized with the 2.3-kb ClaI/EcoRI DNA fragment containing the TA29 gene [(C)].

(B) Hybridization of the TSJT1 gene with anther and leaf ^{32}P-nuclear RNAs. A plasmid (TA29Eco6.6R) representing the right half of the λTA29 phage DNA (Figure 10A) was digested with PstI and EcoRI, transferred to nytran, and hybridized with ^{32}P-nuclear RNA synthesized in vitro from either stage 3 anther nuclei or leaf nuclei (see Methods). The band labeled with a circled asterisk represents an RNA polymerase II transcript that hybridized with the 2.2-kb PstI/EcoRI DNA fragment [(C)], and that was undetectable in the organ system mRNA gel blots shown in Figure 10B. The band labeled with an S represents the TSJT1 nuclear RNA that hybridized with the 3.3-kb PstI fragment containing the TSJT1 gene [(C)]. The band labeled A + S represents TA29 and TSJT1 nuclear RNAs that hybridized with the 1.1-kb EcoRI/PstI fragment that contained sequences from both genes [(C)].

(C) Transcribed TA29 genomic regions. Restriction map and schematic representations of the TA29 and TSJT1 genes were taken from Figure 10A. Bars with diagonal lines and dots represent restriction fragments contained within plasmids TA29Eco6.6L and TA29Eco6.6R, respectively. These bars show regions that hybridized with anther and leaf ^{32}P-nuclear RNAs. A, S, asterisk and circled asterisk represent TA29, TSJT1, and two unidentified RNA polymerase II transcripts, respectively.

data demonstrate that TA29 5′ sequences between −279 and −150 are required to program high levels of transcription within the tapetum.

We delineated the TA29 gene transcriptional control region further by investigating GUS enzyme activity in

TA29/GUS transformants containing only 178 nucleotides of the TA29 5′ region. The chimeric TA29/GUS genes in these transformants and in control transformants with 279 nucleotides of the TA29 5′ region are schematically represented in Figure 13A. Figure 13B shows that, as predicted, intense blue color resulting from GUS enzyme activity was visualized within the tapetal cells of stage 4 anthers containing a TA29/GUS gene with 279 nucleotides of TA29 5′ sequences. No color was observed in the tapetal cells of stage 1 and stage 6 anthers of the same transformants (Figure 13B). By contrast, no detectable enzyme activity was visualized at any developmental stage within the tapetum of transformants containing a chimeric TA29/GUS gene with only 178 nucleotides of the TA29 5′ region (data not shown). Nor was there any GUS enzyme activity visualized within the roots, stems, leaves, and cotyledons of germinated seedlings containing either the −279 or the −178 TA29/GUS genes (data not shown). Together, these data indicate that sequences between −279 and −178 relative to the TA29 gene transcription start site are required for both temporal specificity (Figures 4A and 4C) and tapetal-cell specificity (Figures 5G to 5I) during anther development.

We fused selected portions of the TA29 gene −279 5′ region with a GUS gene that contained a minimal cauliflower mosaic virus (CaMV) promoter (Figure 13A) and then transferred these chimeric TA29/CaMV/GUS genes to tobacco plants to show directly that sequences in this region were sufficient to transcriptionally activate a heterologous promoter in the tapetum. Figures 13C and 13D show that a high level of GUS enzyme activity was visualized within stage 4 anther tapetal cells of TA29/CaMV/GUS gene transformants containing TA29 5′ nucleotides −279 to −85 (Figure 13C) and −207 to −85 (Figure 13D). By contrast, Figure 13E shows that no GUS activity was visualized within tapetal cells of control transformants containing a GUS gene with the minimal CaMV promoter (Figure 13A). Nor was GUS activity visualized in the tapetum of TA29/CaMV/GUS transformants with TA29 5′ nucleotides −178 to −85 (Figure 13A) (data not shown). Surprisingly, TA29/CaMV/GUS transformants containing the −279 to −178 TA29 5′ region (Figure 13A) did not have detectable GUS activity above control levels (Figure 13E) in their tapetal cells (data not shown). We conclude from these data that a 122-bp TA29 5′ region between nucleotides −207 and −85 (Figures 10A and 13A) contains sequences sufficient to program TA29 gene tapetal-specific transcription during the tobacco life cycle. These transcriptional control sequences either exist as separate elements within the −207 to −178 and −178 to −85 regions, or extend as one domain across nucleotide −178 into each region, or both.

The Tapetum Functions Autonomously during Phase 2 of Anther Development

We fused a 1.5-kb TA29 5′ region containing the tapetal cell transcriptional control sequences (Figure 10A; Mariani
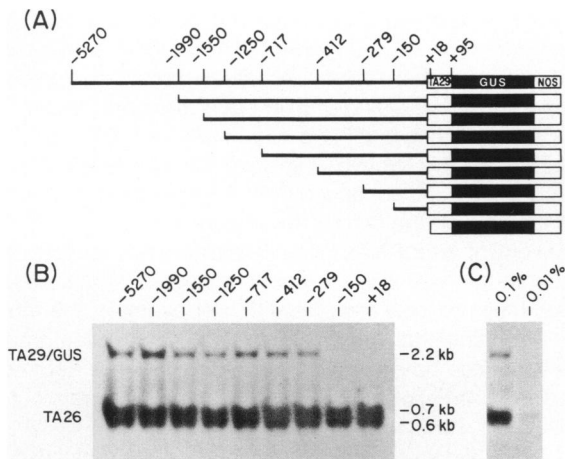
Figure 12. Localization of the Tapetal-Specific TA29 Gene Transcriptional Control Region.

Chimeric TA29/GUS genes containing different amounts of the TA29 gene 5′ region (Figure 10A) were transferred to tobacco plants as described in Methods. Approximately 150 stage 3 anthers (0.4 g) from each of five different transformants per deletion were pooled, and their polysomal poly(A) mRNAs were isolated as outlined in Methods. One microgram of mRNA from each deletion pool was fractionated on denaturing agarose gels, transferred to nytran, and hybridized with a mixture of ^{32}P-anti-mRNAs synthesized from TA26 and GUS plasmids.

(A) Schematic representation of the 5′ TA29 region in each chimeric TA29/GUS gene. End points of the +18, −150, −279, −412, and −717 deletions were determined directly by DNA sequence analysis. The remainder were estimated by agarose gel electrophoresis relative to known marker DNAs.

(B) GUS and TA26 mRNA levels in anthers of pooled transformants containing a TA29/GUS gene.

(C) Reconstruction lanes calibrating the TA29/GUS deletion mRNA gel blots. GUS and TA26 mRNAs were synthesized in vitro. Equal mass amounts of each mRNA were mixed, fractionated on denaturing agarose gels, transferred to nytran, and hybridized with TA26 and GUS ^{32}P-anti-mRNAs as outlined in Methods. The 0.1% and 0.01% reconstruction lanes contained 10^{-3} μg and 10^{-4} μg each of GUS and TA26 mRNAs, respectively. All TA29/GUS and reconstruction RNA gel blots were exposed for the same time period (4 hr).

et al., 1990) with the cytotoxic diphtheria toxin A-chain (DTA) gene (see Methods) to (1) determine whether tapetal cell specification occurred before TA29 gene transcriptional activation, and (2) to determine whether destruction of the tapetum had any effect on the differentiation and/or function of other anther cells. We transferred the chimeric TA29/DTA gene to tobacco cells and regenerated seven independent transformants (see Methods). DNA gel blot studies and Kn^r gene segregation patterns demonstrated that each transformant had a single, unrearranged copy of the TA29/DTA gene (data not shown).

Figure 2 shows that anther development in plants with the chimeric TA29/DTA gene (Figure 2B) was identical to untransformed wild-type plants (Figure 2A) from stages −7 to −2. The bright-field photographs shown in Figure 14 indicate that stage −2 anthers of control plants (Figure 14A) and TA29/DTA plants (Figure 14D) were indistinguishable and that major anther tissues such as the epidermis, endothecium, connective, and tapetum had differentiated, as well as the microspore mother cells. By contrast, Figures 14B, 14C, 14E, and 14F show that both tapetal and microspore mother cells were abnormal in appearance in stage −1 TA29/DTA anthers (Figure 14E) and that complete tapetum destruction and pollen sac collapse occurred by stage 1 (Figure 14F). Figure 2B shows that subsequent stages of anther development in plants with the TA29/DTA gene were identical to those of the control plants (Figure 2A). The anthers enlarged, the connective and stomium degenerated, and the anthers dehisced. The only difference between plants with the TA29/DTA gene and wild-type plants was the absence of pollen grains at dehiscence; that is, the TA29/DTA plants were male sterile. We conclude from these data that the TA29 gene is activated after tapetal cell differentiation has occurred during a period when meiosis is taking place (Table 1) and that destruction of the tapetum has no effect on anther differentiation and/or function later in development.

DISCUSSION

Gene Expression Is Temporally and Spatially Regulated during Anther Development

We have identified several different prevalent mRNAs that are present either exclusively (e.g., TA13, TA29) or at elevated levels (e.g., TA20, TA26) in the anther (Figure 3). These experiments complement our previous results (Kamalay and Goldberg, 1980, 1984) and those of others (Stinson et al., 1987; Gasser et al., 1988; Ursin et al., 1989; Twell et al., 1990; van Tunen et al., 1990) and indicate that the differentiated state of the anther is associated with the expression of unique genes. A major aspect of the results presented here is the finding that different temporal and spatial gene expression programs occur during anther development and that these programs correlate with the differentiation of specific tissues and cell types.

A schematic representation of the gene expression programs that we have identified during anther development is presented in Figure 15. First, the TA13, TA26, TA29, TA32, and TA36 mRNAs accumulate coordinately during early phase 2 of anther development, decay before the stage when microspore nuclei divide in the pollen sac (Figure 4 and Table 1), and are localized exclusively within the tapetum (Figure 5). Second, the TA56 mRNA accumulates later than the tapetal-specific mRNAs, persists
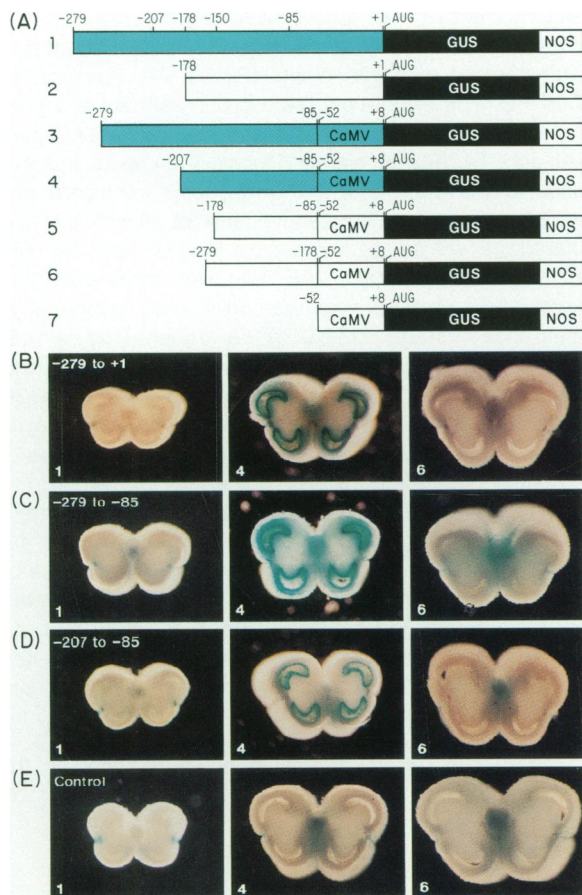
Figure 13. Identification of Transcriptional Control Sequences within the TA29 Gene −279 5′ Region.

DNA fragments representing different segments of the TA29 gene −279 5′ region (Figure 10A) were fused with either the GUS gene coding region or a chimeric GUS gene containing a CaMV minimal promoter (see Methods) and transferred to tobacco plants as outlined in Methods. Stage 1, 4, and 6 anthers from each transformant were harvested and assayed for GUS enzyme activity as outlined in Methods. We examined eight individual transformants per chimeric TA29 gene construction. Although GUS levels varied, the qualitative pattern was the same in each transformant.
(A) Schematic representation of the TA29 gene −279 5′ region in each chimeric TA29/GUS gene. Blue 5′ regions represent chimeric genes that produced the tapetal-specific GUS expression patterns shown in **(B)** to **(D)**.
(B) to **(E)** Localization of GUS enzyme activity in transformants with TA29/GUS genes 1 [**(B)**], 3 [**(C)**], 4 [**(D)**], and 5, 6, and 7 [**(E)**] as schematically diagrammed in **(A)**. 1, 4, and 6 refer to stages of anther development.

throughout phase 2 of anther development, and decays just before dehiscence and flower opening (Figures 4 and 6). The TA56 mRNA is localized within the stomium, the connective, and the circular cell cluster between the stomium and connective (Figure 6). TA56 mRNA localization within these anther regions, however, occurs in a precise temporal cascade—first circular cell cluster, next stomium, and then connective (Figure 15). Finally, the TA20 mRNA accumulates to a relatively high level before stage 1 (Figure 4) and is localized continuously in the epidermis, stomium, wall layers, and the connective (Figure 7).

Several of the mRNAs investigated here encode proteins that correlate well with the known functions of the cells in which they are localized (Table 2). For example, the tapetum is essential for the differentiation of the pollen grains and produces both proteins and lipids that are secreted into the pollen sac and form part of the pollen grain outer wall (Vasil, 1967; Heslop-Harrison, 1975). The TA13/29 and TA32/36 tapetal-specific mRNAs encode putative glycine-rich cell wall proteins and lipid transfer proteins, respectively (Table 2). These proteins are excellent candidates for molecules that play a critical role in tapetum physiological processes. By contrast, the TA56 mRNA encodes a protein similar to the thiol endopeptidases that are present in germinating cotyledons (Mitsuhashi and Minamikawa, 1989) and senescing leaves (Miller and Huffaker, 1982). The appearance of the TA56 mRNA in the connective, stomium, and circular cell cluster just before their degeneration (Figure 6) suggests that the TA56 thiol endopeptidase may aid in the degenerative process by either activating hydrolytic enzymes that degrade cellular macromolecules, or by functioning as a hydrolytic enzyme, or both.

A Mosaic of Regulatory Programs Operate in the Anther

Our results suggest that genes expressed in the anther are regulated, in part, by a mosaic of control programs that are partitioned with respect to both cell type and developmental time within the anther. For example, the TA20, TA29, and TA56 genes respond differentially to regulatory signals present within the wall layers, tapetum, and circular cell cluster, respectively (Figure 15). By contrast, the TA20 and TA56 genes both respond to signals present within the stomium and connective, but are coexpressed within these tissues only during specific developmental periods (Figure 15). We showed directly using runoff transcription studies (Figure 11) and transformation experiments with chimeric genes (Figures 12 to 14) that the tapetal-specific expression of the TA29 gene is controlled at the transcriptional level. Assuming that the other anther-specific genes that we have investigated are also regulated by transcriptional processes (Kamalay and Goldberg, 1984), our results suggest that the mRNA localization patterns that we have observed reflect the distribution of transcription factors capable of activating these genes during anther development.
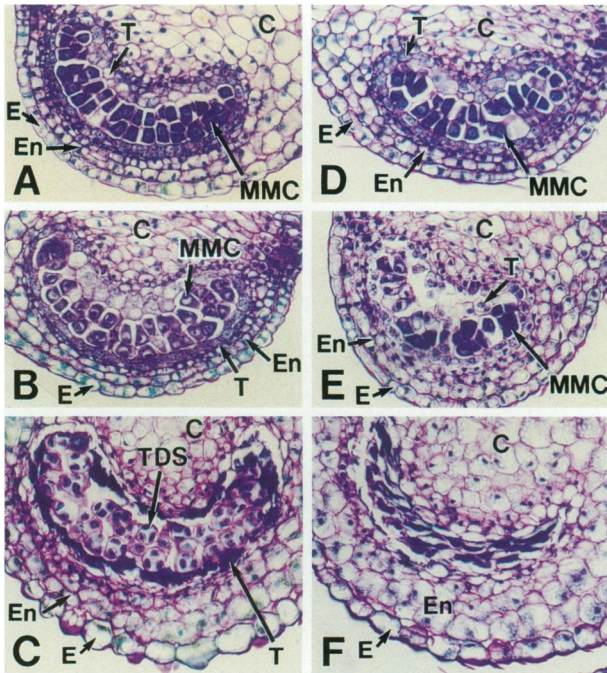
Figure 14. Bright-Field Photographs of Anthers from Untransformed Plants and Plants Containing a Chimeric TA29/DTA Gene.

Anthers were fixed, embedded in paraffin, and sliced into 10-μm sections as outlined in the legend to Figure 2 and in Methods. C, connective; E, epidermis; En, endothecium; MMC, microspore mother cells; T, tapetum; TDS, tetrads.

(A) to **(C)** Bright-field photographs of untransformed anthers at stage −2 [**(A)**], −1 [**(B)**], and 1 [**(C)**]. Magnification factor was ×160.

(D) to **(F)** Bright-field photographs of anthers containing the TA29/DTA gene at stages −2 [**(D)**], −1 [**(E)**], and 1 [**(F)**]. Magnification factor was ×160.

The gene expression programs that we have identified take place within sporophytic tissues and probably represent only a fraction of the regulatory programs that occur during anther development. Other anther-specific gene expression programs have been identified that occur within the developing male gametophyte or pollen grain (Stinson et al., 1987; Mascarenhas, 1988; Hanson et al., 1989; Ursin et al., 1989; Brown and Crouch, 1990; Twell et al., 1990). In each case, these programs deal with the prevalent mRNA sets that are regulated during phase 2 of anther development and represent only a small fraction of the thousands of anther-specific mRNAs known to occur (Kamalay and Goldberg, 1980, 1984). For example, the TA29 mRNA constitutes 0.2% of the stage 3 anther mRNA mass as a whole (Table 2) and on a cell basis represents a much larger percentage of the tapetal mRNA mass (Figure 5). By contrast, a typical rare class anther mRNA constitutes only 10^{-3}% of the anther mRNA mass (Kamalay and

Goldberg, 1980), or approximately the level of the TSJT1 mRNA in the anther (Figure 10C). No information exists at the present time regarding the regulation of genes encoding rare mRNAs during anther development. Nor is there any information regarding gene expression programs that operate during phase 1 of anther development when major histodifferentiation events occur (Figure 2). Nevertheless, the cell-specific mRNAs identified by us and by others (Ursin et al., 1989) provide useful markers for dissecting the regulatory pathways that control the specification of different cell types during anther development.

Several Coordinately Regulated Tapetal-Specific Genes Have Been Identified

One of the most striking aspects of our results is the identification of several genes that are coordinately expressed with respect to both time and cell type during anther development. Figures 4 and 5 show that the TA13, TA26, TA29, TA32, and TA36 mRNAs accumulate and decay in the same temporal sequence during anther development and are localized collectively within the tapetum. Other anther-specific mRNAs (e.g., TA1, TA51) have identical accumulation and decay programs and are probably localized within the tapetum as well (Figure 4).

At least one tapetal-specific gene, that encoding the TA29 mRNA, does not appear to be expressed detectably at any other time of the sporophytic life cycle. No detectable TA29 mRNA is present at the level of RNA gel blots in heterologous vegetative and floral organ systems (Figure 3). Transformed plants containing cytotoxic genes controlled by the TA29 5′ gene region are indistinguishable from control plants except that they are male sterile as a consequence of tapetal cell destruction (Figure 14; Mariani et al., 1990). Finally, we have not detected these transcripts or their TA13 relatives in any other organ system using the polymerase chain reaction (PCR) (C. Mariani, M. De Bueckeleer, and R.B. Goldberg, unpublished results). By contrast, other tapetal-specific mRNAs are present in heterologous organs. For example, the RNA gel blot studies shown in Figure 3 indicate that the TA26 mRNA is present in the leaf, and PCR studies have shown that the TA32 and TA36 mRNAs are present at low levels in the leaf, stem, and root (C. Mariani, M. De Bueckeleer, and R.B. Goldberg, unpublished results). We also cannot exclude the possibility that tapetal-specific genes, including those encoding the TA13 and TA29 mRNAs, are expressed during the gametophytic phase of the life cycle, although in situ hybridization experiments have not detected these mRNAs within developing pollen grains (data not shown). We conclude that several different genes investigated form part of a regulatory network that is activated in the tapetum and that some of these tapetal-specific genes are linked to additional regulatory circuits that are active at other times of the life cycle.
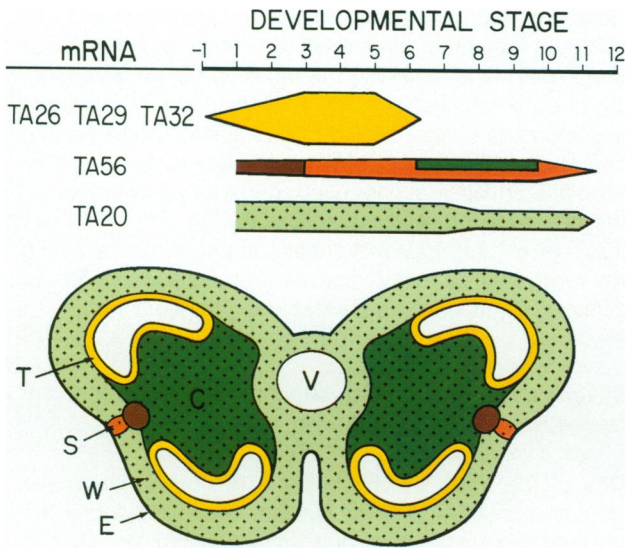
Figure 15. Temporal and Spatial Regulation of mRNAs during Anther Development.

Data represent a summary of the RNA blot and in situ hybridization experiments shown in Figures 4 to 7. The tapering in each colored bar shows periods when the mRNA accumulates or decays, and the bar thickness approximates the prevalence of each set averaged over the entire anther mRNA population (Table 2). The color of each bar corresponds with the anther region in which each mRNA is localized. Three colors were used for TA56 because this mRNA is localized in several anther regions at different developmental periods. C, connective; S, stomium; T, tapetum; V, vascular bundle; W, wall.

Experiments with the chimeric TA29/DTA gene (Figure 14) indicated that the TA29 gene is activated transcriptionally after the tapetum has differentiated during a period when meiosis occurs in the microsporangia (Figure 14 and Table 1). We do not know how many other tapetal-specific genes are also activated at this time. However, the transcriptional activation of the TA29 gene occurs close to the developmental stage when tapetal cell specification takes place within the anther (Figure 2). Identification of transcription factors that regulate this gene and others in the tapetal-specific regulatory network should provide entry into the tapetum differentiation pathway close to the period when critical specification decisions occur.

A Tapetal-Specific Regulatory Domain Has Been Identified

Dissection of the TA29 5′ region by both deletion experiments (Figures 12 and 13) and gain of function experiments with a heterologous promoter (Figure 13) has identified a 122-bp 5′ region (−207 to −85) that is both necessary and sufficient to program tapetal-specific

expression within the anther. Sequences within this domain are required to activate TA29 gene transcription within the correct organ system and cell type and at the appropriate time of the tobacco life cycle. Activation of the TA29 gene probably requires transcription factors that are either present exclusively in the tapetum or are present in an active state only in the tapetum. Tapetal-specific transcription factors must be highly conserved because the TA29 gene 5′ region can program tapetal-specific expression of both GUS and RNase genes in distantly related oilseed rape plants (Mariani et al., 1990). Comparisons of the TA29 −207 to −85 regulatory domain with the TA36 tapetal-specific 5′ gene region did not reveal any significant DNA sequence homologies (J. Seurinck, A.M. Koltunow, and R.B. Goldberg, unpublished results). What the exact tapetal-specific cis elements are and how factors interact with these elements to activate the transcription of tapetal-specific genes remain to be determined.

Chimeric Cytotoxic Genes Can Be Used To Study Cell Interaction Processes during Anther Development

The mechanisms by which different cells and tissues form during anther development are not known. As shown in Figures 2 and 14, cells that serve as precursors to major tissues appear at specific positions within the anther. For example, archesporial cells arise simultaneously in each corner of the anther, and these archesporial cells differentiate into the microsporangia and their surrounding tissues such as the tapetum and endothecium (Vasil, 1967; Esau, 1977; Mascarenhas, 1988). By contrast, the vascular tissues differentiate within the center of the anther (Figure 2). Thus, specific regions, or territories, are established early in anther development within which unique histodifferentiation events occur. In some cases, other tissues (e.g., stomium) form at the boundaries of these territories later in anther development (Figures 2 and 6).

Cell lineage studies (Satina and Blakeslee, 1941) showed that after the stamen primordia are specified, the epidermis is derived from the L1 floral meristem layer. Other anther tissues are formed from the L2 or L3 layers, or both (Satina and Blakeslee, 1941). For example, the tapetum is formed from both the archesporial lineage that is derived from the L2 layer and the connective lineage that is established from L3. The specification of the tapetum from two lineages within each microsporangia territory suggests that cell position is more critical than cell ancestry in the anther histospecification process.

No information exists on whether different anther cells and tissues are induced by signals from contiguous regions of a territory, or are specified autonomously by sequestering morphogenetic factors during divisions of the L1, L2, and L3 layers, or both. We have shown in this paper (Figures 2 and 14) and elsewhere (Mariani et al., 1990) that cytotoxic genes controlled by the TA29 gene 5′ region

(Figure 13) can selectively destroy the tapetum during anther development. Both the TA29/DTA gene (Figure 14) and two different TA29/RNase genes (Mariani et al., 1990) cause tapetal cell breakdown between stages −1 and 1 of tobacco anther development. Destruction of the tapetum by either DTA or RNase does not affect the function and/or differentiation of anther cell types at later developmental stages (Figures 2 and 14; Mariani et al., 1990). We infer from these observations that the tapetum functions autonomously during phase 2 of anther development. We do not know, of course, what effect tapetal cell loss at an earlier period would have on differentiation events that occur within contiguous cells of the same territory. Use of cell-specific gene regulatory domains that can activate cytotoxic genes early in anther development should, in principle, be able to address the role of cell-cell interactions during the anther differentiation process. Clearly, the mechanisms that control cell type specification during anther development and how unique gene sets are activated coordinately within these cell types remain major unanswered questions.

METHODS

Growth of Plants

Tobacco plants (Nicotiana tabacum cv Samsun) and other Nicotiana species (N. tomentosiformis, N. sylvestris) were grown in the greenhouse. Characteristics of plants and organ systems used for RNA preparations were described elsewhere (Kamalay and Goldberg, 1980; Cox and Goldberg, 1988).

Polysomal mRNA Isolation

Polysomal poly(A) mRNAs from tobacco vegetative and floral organ systems were isolated according to the procedures described by Cox and Goldberg (1988).

DNA Isolation and Labeling

Tobacco leaf nuclear DNAs, as well as plasmid and phage DNAs, were isolated as outlined in Jofuku and Goldberg (1988). Plasmid and phage DNAs were labeled by nick translation under conditions specified by Bethesda Research Laboratories. Single-copy DNA sequences were labeled by gap translation as described previously (Goldberg et al., 1978; Kamalay and Goldberg, 1980; Okamuro and Goldberg, 1985).

Isolation of Single-Copy DNA

Unlabeled single-copy DNA sequences were isolated from total DNA by two cycles of renaturation and hydroxyapatite fractionation to Cots 2000 and 200, respectively (Goldberg et al., 1981). The final nonreassociated single-copy DNA fraction represented 4% of the starting DNA, and was reassociated to Cot 7000 to generate networks for the gap translation labeling reaction (Goldberg et al., 1978, 1981; Kamalay and Goldberg, 1980; Okamuro and Goldberg, 1985).

Solution DNA Hybridization Studies

Procedures used for DNA-excess hybridization experiments with single-copy DNA and cDNA have been described extensively elsewhere (Goldberg et al., 1978, 1981; Kamalay and Goldberg, 1980; Okamuro and Goldberg, 1985). Computer analysis of the hybridization kinetics was carried out as described by Pearson et al. (1977), using a program that was modified for use on an IBM personal computer by June Baumer of the UCLA Biology Department.

Gel Blot Studies

DNA and RNA gel blot studies were carried out according to previously published procedures (Jofuku and Goldberg, 1988, 1989). RNA dot blot experiments were performed according to Barker et al. (1988).

Light Microscopy of Anther and Pistil Sections

Anthers and pistils were dissected from flower buds at the relevant developmental stages and fixed with glutaraldehyde as described by Cox and Goldberg (1988). The fixed floral organs were dehydrated, cleared of chlorophyll, embedded in paraffin, and sliced into 10-μm sections as outlined previously (Cox and Goldberg, 1988). The sections were stained with 0.05% toluidine blue, and photographed with Kodacolor Gold100 film with bright-field illumination as described (Cox and Goldberg, 1988; Perez-Grau and Goldberg, 1989). Color prints were produced by Village Photo (Westwood, CA) using an automated developing and printing process. In some cases, these prints were spliced together to reconstruct the entire organ visualized in the microscopic field.

In Situ Hybridization Studies

In situ hybridization studies with paraffin-embedded organ system sections were carried out exactly as described by Cox and Goldberg (1988) and Perez-Grau and Goldberg (1989).

Synthesis of Single-Stranded Probes

Labeled and unlabeled single-stranded RNAs were synthesized using the pGEM transcription system (Promega Biotec). ^{35}S-RNA and ^{32}P-RNA probes were used for in situ and gel blot hybridization studies, respectively.

Runoff Transcription Studies

Synthesis of ^{32}P-RNA in isolated nuclei was carried out as described by Walling et al. (1986) and Cox and Goldberg (1988). To

prevent contamination of anther nuclei with developing pollen grains, the anther homogenates were passed through a 20-μm nylon mesh screen.

R-Loop Analysis

R-loops were formed between λTA29 phage DNA and organ system mRNAs as described by Fischer and Goldberg (1982) and Jofuku and Goldberg (1988). Procedures for visualizing the R-loops in the transmission electron microscope were described previously (Fischer and Goldberg, 1982).

Construction and Screening of Anther cDNA Library

A stage 6 anther cDNA library was constructed in pBR329 (Covarrubias and Bolivar, 1982) according to the RNase H procedure of Gubler and Hoffman (1983). Complementary DNA clones representing mRNAs present exclusively or at elevated levels in the anther were identified by screening replica plates of the anther library separately with stage 6 anther ^{32}P-cDNA and a mixture of leaf, root, stem, pistil (stage 6), and petal (stage 12) ^{32}P-cDNAs. Bacterial colonies were screened by the hybridization procedures of Grunstein and Hogness (1975) and Hanahan and Meselson (1980).

Construction and Screening of Tobacco Genome Library

Tobacco leaf DNA sequences were cloned in the λCharon 32 vector (Loenen and Blattner, 1983) according to the procedure of Jofuku and Goldberg (1988). Approximately 8×10^5 independent phage isolates were plated and amplified to form a permanent library, and greater than 99% of these phage were recombinants. The λTA29 genomic clone was isolated from this library by the plaque hybridization procedures described by Jofuku and Goldberg (1988).

Scanning Electron Microscopy

Flower buds and anthers were fixed and prepared for scanning electron microscopy according to the procedure of Irish and Sussex (1990). Samples were examined in an ETEC autoscan scanning electron microscope (ETEC Corporation, Hayward, CA) with an acceleration voltage of 10 kV.

Histochemical Assay for GUS Enzyme Activity

Histochemical staining for GUS enzyme activity was carried out according to the procedure of Jefferson et al. (1987), with minor additions to optimize visual detection of GUS activity in anthers. In brief, anthers were sliced into 2-mm pieces and fixed by vacuum infiltration for 15 min in 0.1 M sodium phosphate buffer (pH 7.0) containing 0.1% formaldehyde, 0.1% Triton X-100, and 0.1% β-mercaptoethanol. The fixed anthers were then rinsed extensively with 0.1 M sodium phosphate buffer (pH 7.0) containing 0.1% β-mercaptoethanol, followed by a rinse with 0.05 M sodium phosphate buffer (pH 7.0) plus 0.1% β-mercaptoethanol.

GUS reactions were carried out at 37°C in 0.05 M sodium phosphate buffer (pH 7.0) containing 0.1% Triton X-100, 0.1% β-mercaptoethanol, and 0.001 M 5-bromo-4-chloro-3-indolylglucuronide (X-gluc). After a visible histochemical reaction occurred, the anthers were fixed in 5% formaldehyde, 5% acetic acid, and 20% ethanol for 2 hr, and then cleared of chlorophyll by shaking in 50% ethanol for 2 hr and then in 100% ethanol overnight. Anthers were photographed with Kodacolor Gold100 film using an Olympus SZH stereo microscope with dark-field illumination.

Gene Fusions Used for Transformation Studies

TA29 gene 5' regions were inserted into a pGV1500-derived Ti-plasmid cointegration vector (Deblaere et al., 1987) that was modified to contain the *Escherichia coli* GUS gene (Jefferson et al., 1987). Deletions of the TA29 gene 5' region were generated from a 5.7-kb SalI/HindIII fragment (nucleotides −5670 to +95; Figure 10A) using the exonuclease III procedure of Henikoff (1987). The −279 to +1 TA29 transcriptional control region (Figure 13) was inserted directly into the pGV1500 GUS vector. By contrast, DNA fragments representing portions of this region were inserted into a similar GUS vector that contained the CaMV 35S gene minimal promoter (nucleotides −52 to +8; Benfey et al., 1990a, 1990b). The chimeric TA29/DTA gene was constructed exactly as described by Mariani et al. (1990) using a 5' TA29 gene fragment containing nucleotides −1477 to +51 (Figure 10A) and the DTA coding sequence (Greenfield et al., 1983; Maxwell et al., 1986; Palmiter et al., 1987).

Transformation of Tobacco Plants

Chimeric TA29/GUS genes were transferred from the pGV1500 vector to the disarmed *Agrobacterium* pGV2260 Ti-plasmid (Deblaere et al., 1987), and tobacco leaf discs were transformed according to the procedure of Horsch et al. (1985) using kanamycin selection.

REFERENCES

Barker, S.J., Harada, J.J., and Goldberg, R.B. (1988). Cellular localization of soybean storage protein mRNA in transformed tobacco seeds. Proc. Natl. Acad. Sci. USA **85,** 458–462.

Benfey, P.N., Ren, L., and Chua, N.-H. (1990a). Tissue-specific expression from CaMV 35S enhancer subdomains in early stages of plant development. EMBO J. **9,** 1677–1684.

Benfey, P.N., Ren, L., and Chua, N.-H. (1990b). Combinational and synergistic properties of CaMV 35S enhancer subdomains. EMBO J. **9,** 1685–1696.

Bouillon, P., Drischel, C., Vergnolle, C., Duranton, H., and Kader, C.-J. (1987). The primary structure of spinach leaf phospholipid transfer protein. Eur. J. Biochem. **166,** 387–391.

Bowman, J.L., Smyth, D.R., and Meyerowitz, E.M. (1989). Genes directing flower development in *Arabidopsis*. Plant Cell **1,** 37–52.

Brown, S.M., and Crouch, M.L. (1990). Characterization of a gene family abundantly expressed in *Oenothera organensis* pollen that shows sequence similarity to polygalacturonase. Plant Cell **2,** 263–274.

Carpenter, R., and Coen, E.S. (1990). Floral homeotic mutations produced by transposon-mutagenesis in *Antirrhinum majus*. Genes Dev. **4,** 1483–1493.

Condit, C.M., and Meagher, R.B. (1986). A gene encoding a novel glycine-rich structural protein of *Petunia*. Nature **323,** 178–181.

Covarrubias, L., and Bolivar, F. (1982). Construction and characterization of new cloning vehicles. VI. Plasmid pBR329, a new derivative of pBR328 lacking the 428 base pair inverted duplication. Gene **17,** 79–89.

Cox, K.H., and Goldberg, R.B. (1988). Analysis of plant gene expression. In Plant Molecular Biology: A Practical Approach, C.H. Shaw, ed (Oxford: IRL Press), pp. 1–34.

Deblaere, R., Reynaerts, A., Höfte, H., Hernalsteens, J.-P., Leemans, J., and Van Montagu, M. (1987). Vectors for cloning in plant cells. Methods Enzymol. **153,** 277–292.

Drews, G.N., and Goldberg, R.B. (1989). Genetic control of flower development. Trends Genet. **5,** 256–261.

Esau, K. (1977). Anatomy of Seed Plants. (New York: John Wiley).

Fischer, R.L., and Goldberg, R.B. (1982). Structure and flanking regions in soybean seed protein genes. Cell **29,** 651–660.

Gasser, C.S., Smith, A.G., Budelier, K.A., Hinchee, M.A., McCormick, S., Horsch, R.B., Shah, D.M., and Fraley, R.T. (1988). Isolation of differentially expressed genes from tomato flowers. In Temporal and Spatial Regulation of Plant Genes, D.P.S. Verma and R.B. Goldberg, eds (Vienna: Springer-Verlag), pp. 85–96.

Goldberg, R.B. (1988). Plants: Novel developmental processes. Science **240,** 1460–1467.

Goldberg, R.B., Hoschek, G., Kamalay, J.C., and Timberlake, W.E. (1978). Sequence complexity of nuclear and polysomal RNA in leaves of the tobacco plant. Cell **14,** 123–131.

Goldberg, R.B., Hoschek, G., Ditta, G.S., and Breidenbach, R.W. (1981). Developmental regulation of cloned superabundant embryo mRNAs in soybean. Dev. Biol. **83,** 218–231.

Goldberg, R.B., Hoschek, G., and Vodkin, L.O. (1983). An insertion sequence blocks the expression of a soybean lectin gene. Cell **33,** 465–475.

Goodspeed, T.H. (1954). The Genus *Nicotiana*: Origins, Relationships, and Evolution of its Species in Light of Their Distribution, Morphology, and Cytogenetics. (Watham: Chronica Botanica).

Greenfield, L., Bjorn, M.J., Horn, G., Fong, D., Buck, G.A., Collier, R.J., and Kaplan, D.A. (1983). Nucleotide sequence of the structural gene for diphtheria toxin carried by corynebacteriophage *β*. Proc. Natl. Acad. Sci. USA **80,** 6853–6857.

Grunstein, M., and Hogness, D.S. (1975). Colony hybridization: A method for the isolation of cloned DNAs that contain a specific gene. Proc. Natl. Acad. Sci. USA **72,** 3961–3965.

Gubler, U., and Hoffman, B.J. (1983). A simple and very efficient method for generating cDNA libraries. Gene **25,** 263–269.

Hanahan, D., and Meselson, M. (1980). Plamid screening at high colony density. Gene **10,** 63–67.

Hanson, D.D., Hamilton, D.A., Travis, J.L., Bashe, D.M., and Mascarenhas, J.P. (1989). Characterization of a pollen-specific cDNA clone from *Zea mays* and its expression. Plant Cell **1,** 173–179.

Henikoff, S. (1987). Unidirectional digestion with exonuclease III in DNA sequence analysis. Methods Enzymol. **155,** 156–165.

Heslop-Harrison, J. (1975). The physiology of the pollen grain surface. Proc. R. Soc. Lond. B **190,** 275–299.

Horsch, R.B., Fry, J.E., Hoffmann, N.L., Eichholtz, D., Rogers, S.G., and Fraley, R.T. (1985). A simple and general method for transferring genes into plants. Science **227,** 1229–1231.

Irish, V.F., and Sussex, I.M. (1990). Function of the *apetela-1* gene during *Arabidopsis* floral development. Plant Cell **2,** 741–753.

Jefferson, R.A., Kavanagh, T.A., and Bevan, M.W. (1987). GUS fusions: *β*-Glucuronidase is a sensitive and versatile fusion marker in higher plants. EMBO J. **6,** 3901–3907.

Jofuku, K.D., and Goldberg, R.B. (1988). Analysis of plant gene structure. In Plant Molecular Biology: A Practical Approach, C.H. Shaw, ed (Oxford: IRL Press), pp. 37–66.

Jofuku, K.D., and Goldberg, R.B. (1989). Kunitz trypsin inhibitor genes are differentially expressed during the soybean life cycle and in transformed tobacco plants. Plant Cell **1,** 1079–1093.

Kamalay, J.C., and Goldberg, R.B. (1980). Regulation of structural gene expression in tobacco. Cell **19,** 935–946.

Kamalay, J.C., and Goldberg, R.B. (1984). Organ-specific nuclear RNAs in tobacco. Proc. Natl. Acad. Sci. USA **81,** 2801–2805.

Keller, B., Sauer, N., and Lamb, C.J. (1988). Glycine-rich cell wall proteins in bean: Gene structure and association of the protein with the vascular system. EMBO J. **12,** 3625–3633.

Loenen, W.A.M., and Blattner, R.R. (1983). Lambda Charon vectors (Ch 32, 33, 34, and 35) adapted for DNA cloning in recombinant-deficient hosts. Gene **26,** 171–179.

Mariani, C., De Beuckeleer, M., Truettner, J., Leemans, J., and Goldberg, R.B. (1990). Induction of male sterility in plants by a chimeric ribonuclease gene. Nature **347,** 737–741.

Mascarenhas, J.P. (1988). Anther and pollen expressed genes. In Temporal and Spatial Regulation of Plant Genes, D.P.S. Verma and R.B. Goldberg, eds (Vienna: Springer-Verlag), pp. 97–115.

Maxwell, I.H., Maxwell, F., and Glode, L.M. (1986). Regulated expression of a diphtheria toxin A chain gene transferred into

human cells: Possible strategy for inducing cancer cell suicide. Cancer Res. **46**, 4660–4664.

Meyerowitz, E.M., Smyth, D.R., and Bowman, J.L. (1989). Abnormal flowers and pattern formation in floral development. Development **106**, 209–217.

Miller, B.L., and Huffaker, R.C. (1982). Hydrolysis of ribulose-1,5-bisphosphate carboxylase by endoproteinases from senescing barley leaves. Plant Physiol. **69**, 58–62.

Mitsuhashi, W., and Minamikawa, T. (1989). Synthesis and posttranslational activation of sulfhydryl endopeptidase in cotyledons of germinating *Vigna mungo* seeds. Plant Physiol. **89**, 274–279.

Okamuro, J.K., and Goldberg, R.B. (1985). Tobacco single-copy DNA is highly homologous to sequences present in the genomes of its diploid progenitors. Mol. Gen. Genet. **198**, 290–298.

Palmiter, R.D., Behringer, R.R., Quaife, C.J., Maxwell, F., Maxwell, I.H., and Brinster, R.L. (1987). Cell lineage ablation in transgenic mice by cell specific expression of a toxin gene. Cell **50**, 435–443.

Pearson, W.R., Davidson, E.H., and Britten, R.J. (1977). A program for least squares analysis of reassociation and hybridization data. Nucl. Acids Res. **4**, 1727–1737.

Perez-Grau, L., and Goldberg, R.B. (1989). Soybean seed protein genes are regulated spatially during embryogenesis. Plant Cell **1**, 1095–1109.

Raven, P.H., Evert, R.F., and Eichhorn, S.E. (1986). Biology of Plants. (New York: Worth).

Satina, S., and Blakeslee, A.F. (1941). Periclinal chimeras in *Datura stramonium* in relation to development of leaf and flower. Am. J. Bot. **28**, 862–871.

Seurinck, J., Truettner, J., and Goldberg, R.B. (1990). The nucleotide sequence of an anther specific gene. Nucl. Acids Res. **18**, 3403.

Sommer, H., Beltrán, J.-P., Huijser, P., Pape, H., Lönnig, W.-E., Saedler, H., and Schwarz-Sommer, Z. (1990). *Deficiens*, a homeotic gene involved in the control of flower morphogenesis in *Antirrinum majus*: The protein shows homology to transcription factors. EMBO J. **9**, 605–613.

Stinson, J.R., Eisenberg, A.J., Willing, R.P., Pe, M.E., Hanson, D.D., and Mascarenhas, J.P. (1987). Genes expressed in the male gametophyte of flowering plants and their isolation. Plant Physiol. **83**, 442–447.

Takishima, K., Wanatabe, S., Yamada, M., Suga, T., and Mamiya, G. (1988). Amino acid sequences of two non-specific lipid transfer proteins from germinated castor bean. Eur. J. Biochem. **177**, 241–249.

Twell, D., Yamaguchi, J., and McCormick, S. (1990). Pollen specific gene expression in transgenic plants: Coordinate regulation of two different tomato gene promoters during microsporogenesis. Development **109**, 705–713.

Ursin, V.M., Yamaguchi, J., and McCormick, S. (1989). Gametophytic and sporophytic expression of anther-specific genes in developing tomato anthers. Plant Cell **1**, 727–736.

van Tunen, A.J., Mur, L.A., Brouns, G.S., Rienstra, J.-D., Koes, R.E., and Mol. J.N.M. (1990). Pollen- and anther-specific *chi* promoters from petunia: Tandem promoter regulation of the *chiA* gene. Plant Cell **2**, 393–401.

Varner, J.E., and Cassab, G.I. (1988). Cell wall proteins. Annu. Rev. Plant Physiol. Plant Mol. Biol. **39**, 321–353.

Vasil, I.K. (1967). Physiology and cytology of anther development. Biol. Rev. **42**, 327–373.

Walling, L., Drews, G.N., and Goldberg, R.B. (1986). Transcriptional and posttranscriptional regulation of soybean seed protein mRNA levels. Proc. Natl. Acad. Sci. USA **83**, 2123–2127.

Yanofsky, M.F., Ma, H., Bowman, J.L., Drews, G.N., Feldmann, K.L., and Meyerowitz, E.M. (1990). The protein encoded by the *Arabidopsis* homeotic gene *agamous* resembles transcription factors. Nature **346**, 35–39.

Zimmerman, J.L., and Goldberg, R.B. (1977). DNA sequence organization in the genome of *Nicotiana tabacum*. Chromosoma **59**, 227–252.